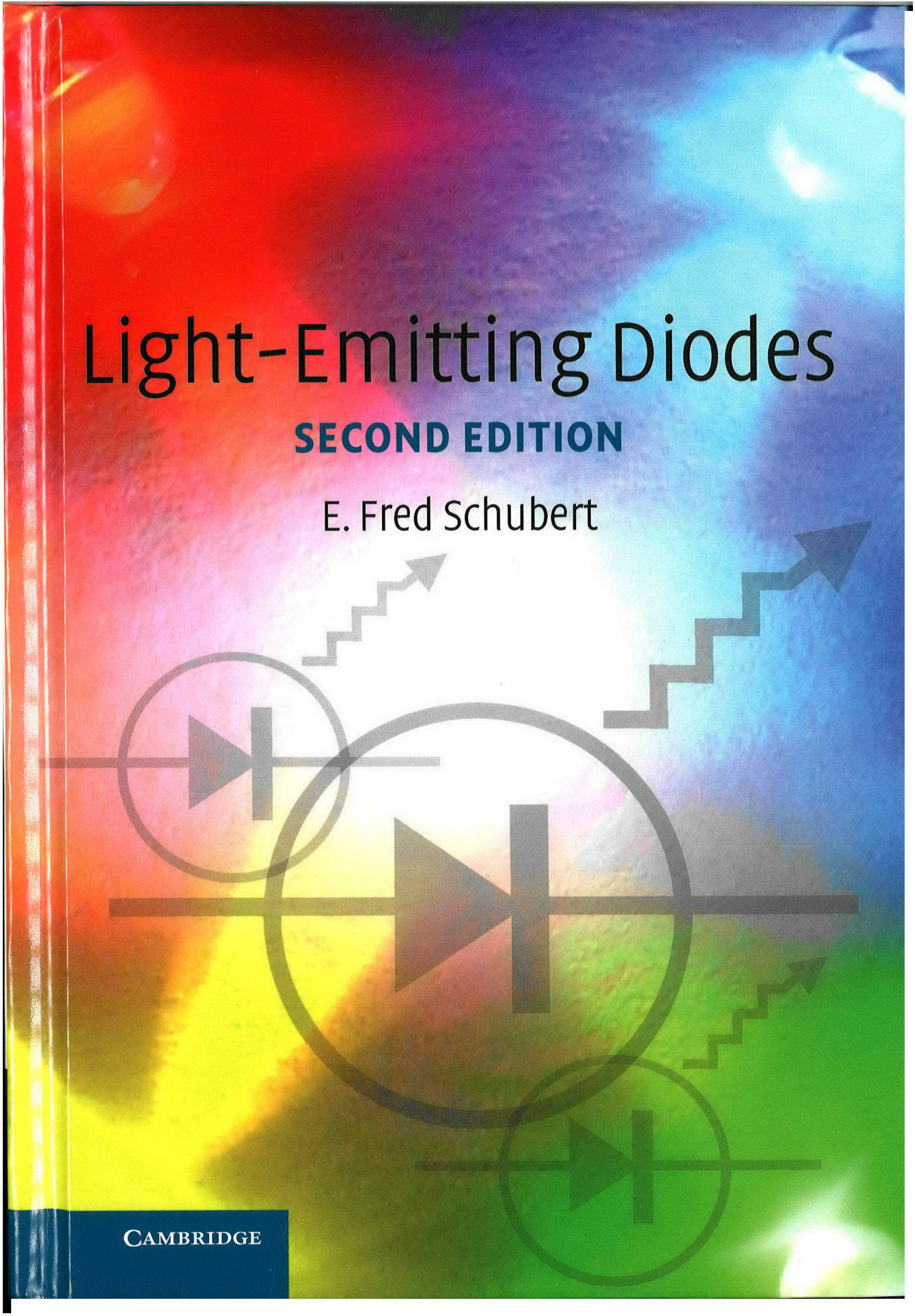
Light-Emitting Diodes
SECOND EDITION
E. Fred Schubert
CAMBRIDGE

LIGHT-EMITTING DIODES

SECOND EDITION

Revised and fully updated, the Second Edition of this textbook offers a comprehensive explanation of the technology and physics of light-emitting diodes (LEDs) such as infrared, visible-spectrum, ultraviolet, and white LEDs made from III–V semiconductors. The elementary properties of LEDs such as electrical and optical characteristics are reviewed, followed by the analysis of advanced device structures.

With nine additional chapters, the treatment of LEDs has been vastly expanded, including new material on device packaging, reflectors, UV LEDs, III–V nitride materials, solid-state sources for illumination applications, and junction temperature. Radiative and non-radiative recombination dynamics, methods for improving light extraction, high-efficiency and high-power device designs, white-light emitters with wavelength-converting phosphor materials, optical reflectors, and spontaneous recombination in resonant-cavity structures, are discussed in detail. Fields related to solid-state lighting such as human vision, photometry, colorimetry, and color rendering are covered beyond the introductory level provided in the first edition. The applications of infrared and visible-spectrum LEDs in silica fiber, plastic fiber, and free-space communication are also discussed. Semiconductor material data, device design data, and analytic formulae governing LED operation are provided.

With exercises, solutions and illustrative examples, this textbook will be of interest to scientists and engineers working on LEDs, and to graduate students in electrical engineering, applied physics, and materials science.

Additional resources for this title are available online at www.cambridge.org/9780521865388.

E. FRED SCHUBERT received his Ph.D. degree with Honors in Electrical Engineering from University of Stuttgart in 1986 and is currently a Wellfleet Senior Constellation Professor of the Future Chips Constellation at Rensselaer Polytechnic Institute. He has made several pioneering contributions to the field of LEDs, including the first demonstration of the resonant-cavity light-emitting diode (RCLED). He has authored or co-authored more than 200 publications including *Doping in III–V Semiconductors* (Cambridge University Press, 1993, 0-521-01784-X) for which he was awarded the VDE Literature Prize. He is inventor or co-inventor of 28 US Patents and a Fellow of the IEEE, APS, OSA, and SPIE. He received the Senior Research Award of the Humboldt Foundation, the Discover Award for Technological Innovation, the RD 100 Award, and Boston University's Provost Innovation Fund Award.

Note: This book contains many figures in which color adds important information. For this reason, all figures are available in color on the Internet at the following websites: <http://www.cambridge.org/9780521865388> and <http://www.LightEmittingDiodes.org>.

LIGHT-EMITTING DIODES

SECOND EDITION

E. FRED SCHUBERT
Rensselaer Polytechnic Institute,
Troy, New York

CAMBRIDGE
UNIVERSITY PRESS

CAMBRIDGE
UNIVERSITY PRESS

University Printing House, Cambridge CB2 8BS, United Kingdom

Cambridge University Press is part of the University of Cambridge.

It furthers the University's mission by disseminating knowledge in the pursuit of education, learning and research at the highest international levels of excellence.

www.cambridge.org
Information on this title: www.cambridge.org/9780521865388

First edition published 2003
Second edition 2006
Second edition reprinted 2007
6th printing 2014

A catalogue record for this publication is available from the British Library

ISBN 978-0-521-86538-8 Hardback

Contents

Preface

During the last four decades, technical progress in the field of light-emitting diodes (LEDs) has been breathtaking. State-of-the art LEDs are small, rugged, reliable, bright, and efficient. At this time, the success story of LEDs still is in full progress. Great technological advances are continuously being made and, as a result, LEDs play an increasingly important role in a myriad of applications. In contrast to many other light sources, LEDs have the potential of converting electricity to light with near-unit efficiency.

LEDs were discovered by accident in 1907 and the first paper on LEDs was published in the same year. LEDs became forgotten only to be re-discovered in the 1920s and again in the 1950s. In the 1960s, three research groups, one working at General Electric Corporation, one at MIT Lincoln Laboratories, and one at IBM Corporation, pursued the demonstration of the semiconductor laser. The first viable LEDs were by-products in this pursuit. LEDs have become devices in their own right and today possibly are the most versatile light sources available to humankind.

The first edition of this book was published in 2003. The second edition of the book is expanded by the discussion of additional technical areas related to LEDs including optical reflectors, the assessment of LED junction temperature, packaging, UV emitters, and LEDs used for general lighting applications. No different than the first edition, the second edition is dedicated to the technology and physics of LEDs. It reviews the electrical and optical fundamentals of LEDs, materials issues, as well as advanced device structures. Recent developments, particularly in the field of III–V nitrides, are also discussed. The book mostly discusses LEDs made from III–V semiconductors. However, much of the science and technology discussed is relevant to other solid-state light emitters such as group-IV, II–VI, and organic emitters. Several application areas of LEDs are discussed in detail, including illumination and communication applications.

Many colleagues and collaborators have provided information not readily available and have given valuable suggestions on the first and second editions of this book. In particular, I am deeply grateful to Enrico Bellotti (Boston University), Jaehee Cho (Samsung Advanced Institute of Technology), George Craford (LumiLeds Corp.), Thomas Gessmann (RPI), Nick Holonyak Jr. (University of Illinois), Jong Kyu Kim (RPI), Mike Krames (LumiLeds Corp.), Shawn Lin (RPI), Ralph Logan (retired, formerly with AT&T Bell Laboratories), Fred Long (Rutgers University), Paul Maruska (Crystal Photonics Corp.), Gerd Mueller (LumiLeds Corp.), Shuji Nakamura (University of California, Santa Barbara), N. Narendran (RPI), Yoshihiro Ohno (National Institute of Standards and Technology), Jacques Pankove (Astralux Corp.), Yongjo Park (Samsung Advanced Institute of Technology), Manfred Pilkuhn (retired, University of Stuttgart, Germany), Hans Rupprecht (retired, formerly with IBM Corp.), Michael Shur (RPI), Cheolsoo Sone (Samsung Advanced Institute of Technology), Klaus Streubel (Osram Opto Semiconductors Corp., Germany), Li-Wei Tu (National Sun Yat-Sen University, Taiwan), Christian Wetzel (RPI), Jerry Woodall (Yale University), and Walter Yao (Advanced Micro Devices Corp.). I would also like to thank my current and former post-doctoral fellows and students for their many significant contributions to this book.

5

LED basics: Optical properties

5.1 Internal, extraction, external, and power efficiencies

The active region of an ideal LED emits *one photon* for *every electron* injected. Each charge quantum-particle (electron) produces one light quantum-particle (photon). Thus the ideal active region of an LED has a *quantum efficiency* of unity. The ***internal quantum efficiency*** is defined as

$$\eta_{\text{int}} = \frac{\text{number of photons emitted from active region per second}}{\text{number of electrons injected into LED per second}} = \frac{P_{\text{int}}/(h\nu)}{I/e} \tag{5.1}$$

where P_{int} is the optical power emitted from the active region and I is the injection current.

Photons emitted by the active region should escape from the LED die. In an ideal LED, all photons emitted by the active region are also emitted into free space. Such an LED has unity *extraction efficiency*. However, in a real LED, not all the power emitted from the active region is emitted into free space. Some photons may never leave the semiconductor die. This is due to several possible loss mechanisms. For example, light emitted by the active region can be reabsorbed in the substrate of the LED, assuming that the substrate is absorbing at the emission wavelength. Light may be incident on a metallic contact surface and be absorbed by the metal. In addition, the phenomenon of *total internal reflection*, also referred to as the *trapped light phenomenon*, reduces the ability of the light to escape from the semiconductor. The light ***extraction efficiency*** is defined as

$$\eta_{\text{extraction}} = \frac{\text{number of photons emitted into free space per second}}{\text{number of photons emitted from active region per second}} = \frac{P/(h\nu)}{P_{\text{int}}/(h\nu)} \tag{5.2}$$

where P is the optical power emitted into free space.

The extraction efficiency can be a severe limitation for high-performance LEDs. It is quite difficult to increase the extraction efficiency beyond 50% without resorting to highly

sophisticated and costly device processes.

The ***external quantum efficiency*** is defined as

$$\eta_{\text{ext}} = \frac{\text{number of photons emitted into free space per second}}{\text{number of electrons injected into LED per second}} = \frac{P/(h\nu)}{I/e} = \eta_{\text{int}}\eta_{\text{extraction}}. \quad (5.3)$$

The external quantum efficiency gives the ratio of the number of useful light particles to the number of injected charge particles.

The ***power efficiency*** is defined as

$$\eta_{\text{power}} = \frac{P}{IV} \quad (5.4)$$

where IV is the electrical power provided to the LED. Informally, the power efficiency is also called the *wallplug efficiency*.

Exercise: ***LED efficiency***. Consider an LED with a threshold voltage of $V_{\text{th}} = E_g/e = 2.0$ V with a differential resistance of $R_s = 20\ \Omega$, so that the I–V characteristic in the forward direction is given by $V = V_{\text{th}} + IR_s$. When the device is operated at 20 mA it emits a light power of 4 mW of energy $h\nu = E_g$. Determine the internal quantum efficiency, the external quantum efficiency, and the power efficiency, assuming that the extraction efficiency is 50%.

5.2 Emission spectrum

The physical mechanism by which semiconductor LEDs emit light is spontaneous recombination of electron–hole pairs and simultaneous emission of photons. The spontaneous emission process is fundamentally different from the stimulated emission process occurring in semiconductor lasers and superluminescent LEDs. Spontaneous recombination has certain characteristics that determine the optical properties of LEDs. The properties of spontaneous emission in LEDs will be discussed in this section.

An electron–hole recombination process is illustrated schematically in Fig. 5.1. Electrons in the conduction band and holes in the valence band are assumed to have the parabolic dispersion relations

$$E = E_C + \frac{\hbar^2 k^2}{2m_e^*} \quad \text{(for electrons)} \quad (5.5)$$

and

$$E = E_V - \frac{\hbar^2 k^2}{2m_h^*} \qquad \text{(for holes)} \qquad (5.6)$$

where m_e^* and m_h^* are the electron and hole effective masses, $\hbar$ is Planck's constant divided by 2π, k is the carrier wave number, and E_V and E_C are the valence and conduction band edges, respectively.

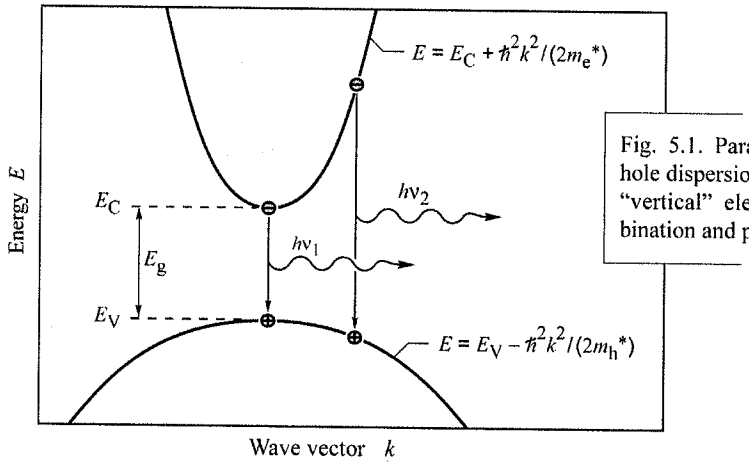

Fig. 5.1. Parabolic electron and hole dispersion relations showing "vertical" electron–hole recombination and photon emission.

The requirement of energy and momentum conservation leads to further insight into the radiative recombination mechanism. It follows from the Boltzmann distribution that electrons and holes have an average kinetic energy of kT. Energy conservation requires that the photon energy is given by the difference between the electron energy, E_e, and the hole energy, E_h, i.e.

$$h\nu = E_e - E_h \approx E_g \,. \qquad (5.7)$$

The photon energy is approximately equal to the bandgap energy, E_g, if the thermal energy is small compared with the bandgap energy $kT << E_g$. Thus the desired emission wavelength of an LED can be attained by choosing a semiconductor material with an appropriate bandgap energy. For example, GaAs has a bandgap energy of 1.42 eV at room temperature and thus GaAs LEDs emit at the infrared wavelength of 870 nm.

It is helpful to compare the average carrier momentum with the photon momentum. A carrier with kinetic energy kT and effective mass m^* has the momentum

$$p = m^*v = \sqrt{2m^*\tfrac{1}{2}m^*v^2} = \sqrt{2m^*kT} \,. \tag{5.8}$$

The momentum of a photon with energy E_g can be derived from the de Broglie relation

$$p = \hbar k = \frac{h\nu}{c} = \frac{E_g}{c} \,. \tag{5.9}$$

Calculation of the carrier momentum (using Eq. 5.8) and the photon momentum (using Eq. 5.9) yields that the carrier momentum is *orders of magnitude larger* than the photon momentum. Therefore the electron momentum cannot change significantly during the transition from the conduction to the valence band. The transitions are therefore "vertical" as shown in Fig. 5.1, i.e. electrons only recombine with holes that have the same momentum or k value.

Using the requirement that electron and hole momenta are the same, the photon energy can be written as the *joint dispersion relation*

$$h\nu = E_C + \frac{\hbar^2 k^2}{2m_e^*} - E_V + \frac{\hbar^2 k^2}{2m_h^*} = E_g + \frac{\hbar^2 k^2}{2m_r^*} \tag{5.10}$$

where m_r* is the reduced mass given by

$$\frac{1}{m_r^*} = \frac{1}{m_e^*} + \frac{1}{m_h^*} \,. \tag{5.11}$$

Using the joint dispersion relation, the joint density of states can be calculated and one obtains

$$\rho(E) = \frac{1}{2\pi^2}\left(\frac{2m_r^*}{\hbar^2}\right)^{3/2}\sqrt{E - E_g} \,. \tag{5.12}$$

The distribution of carriers in the allowed bands is given by the Boltzmann distribution, i.e.

$$f_B(E) = e^{-E/(kT)} \,. \tag{5.13}$$

The *emission intensity* as a function of energy is proportional to the product of Eqs. (5.12) and (5.13),

$$\boxed{I(E) \propto \sqrt{E - E_g}\; e^{-E/(kT)}} \,. \tag{5.14}$$

The lineshape of an LED, as given by Eq. (5.14), is shown in Fig. 5.2. The maximum emission intensity occurs at

$$\boxed{E = E_g + \tfrac{1}{2}kT}. \tag{5.15}$$

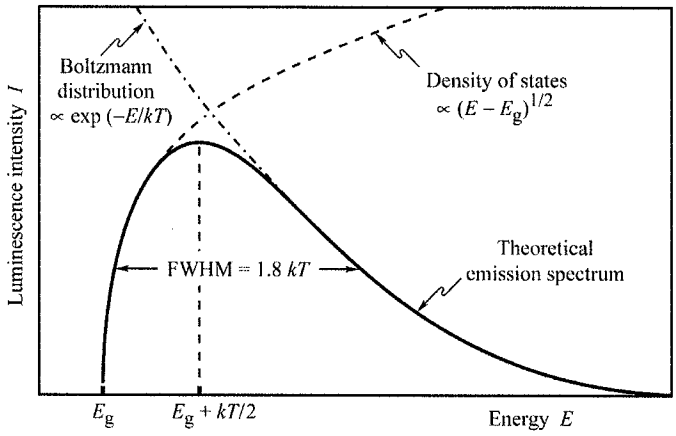

Fig. 5.2. Theoretical emission spectrum of an LED. The full-width at half-maximum (FWHM) of the emission line is $1.8kT$.

The full-width at half-maximum of the emission is

$$\boxed{\Delta E = 1.8kT} \quad \text{or} \quad \boxed{\Delta\lambda = \frac{1.8kT\lambda^2}{hc}}. \tag{5.16}$$

For example, the theoretical room-temperature linewidth of a GaAs LED emitting at 870 nm is $\Delta E = 46$ meV or $\Delta\lambda = 28$ nm.

The spectral linewidth of LED emission is important in several respects. Firstly, the linewidth of an LED emitting in the visible range is relatively narrow compared with the range of the entire visible spectrum. The LED emission is even narrower than the spectral width of a single color as perceived by the human eye. For example, *red* colors range in wavelength from 625 to 730 nm, which is much wider than the typical emission spectrum of an LED. Therefore, LED emission is perceived by the human eye as *monochromatic*.

Secondly, optical fibers are dispersive, which leads to a range of propagation velocities for a light pulse consisting of a range of wavelengths. The material dispersion in optical fibers limits the "*bit rate* × *distance product*" achievable with LEDs.

The spontaneous lifetime of carriers in LEDs in direct-gap semiconductors is of the order of 1–100 ns depending on the active region doping concentration (or carrier concentrations) and the

material quality. Thus, modulation speeds up to 1 Gbit/s are attainable with LEDs.

5.3 The light escape cone

Light generated inside a semiconductor cannot escape from the semiconductor if it is totally internally reflected at the semiconductor–air interface. If the angle of incidence of a light ray is close to normal incidence, light can escape from the semiconductor. However, total internal reflection occurs for light rays with oblique and grazing-angle incidence. Total internal reflection reduces the external efficiency significantly, in particular for LEDs consisting of high-refractive-index materials.

Assume that the angle of incidence in the semiconductor at the semiconductor–air interface is given by ϕ. Then the angle of incidence of the refracted ray, Φ, can be inferred from Snell's law

$$\bar{n}_s \sin\phi = \bar{n}_{air} \sin\Phi \tag{5.17}$$

where $\bar{n}_s$ and $\bar{n}_{air}$ are the refractive indices of the semiconductor and air, respectively. The ***critical angle for total internal reflection*** is obtained using $\Phi = 90°$, as illustrated in Fig. 5.3 (a). Using Snell's law, one obtains

$$\sin\phi_c = \frac{\bar{n}_{air}}{\bar{n}_s} \sin 90° = \frac{\bar{n}_{air}}{\bar{n}_s} \tag{5.18a}$$

and

$$\phi_c = \arcsin \frac{\bar{n}_{air}}{\bar{n}_s} . \tag{5.18b}$$

The refractive indices of semiconductors are usually quite high. For example, GaAs has a refractive index of 3.4. Thus, according to Eq. (5.18), the critical angle for total internal reflection is quite small. In this case, we can use the approximation $\sin\phi_c \approx \phi_c$. The critical angle for total internal reflection is then given by

$$\phi_c \approx \frac{\bar{n}_{air}}{\bar{n}_s} . \tag{5.19}$$

The angle of total internal reflection defines the ***light escape cone***. Light emitted into the cone can escape from the semiconductor, whereas light emitted outside the cone is subject to total internal reflection.

Next, we calculate the surface area of the spherical cone with radius r in order to determine the total fraction of light that is emitted into the light escape cone. The surface area of the calotte-shaped surface shown in Figs. 5.3 (b) and (c) is given by the integral

$$A = \int \mathrm{d}A = \int_{\phi=0}^{\phi_c} 2\pi r \sin\phi \, r \, \mathrm{d}\phi = 2\pi r^2 (1 - \cos\phi_c) \, . \tag{5.20}$$

Let us assume that light is emitted from a point-like source in the semiconductor with a total power of P_{source}. Then the power that can escape from the semiconductor is given by

$$P_{escape} = P_{source} \frac{2\pi r^2 (1 - \cos\phi_c)}{4\pi r^2} \tag{5.21}$$

where $4\pi r^2$ is the entire surface area of the sphere with radius r.

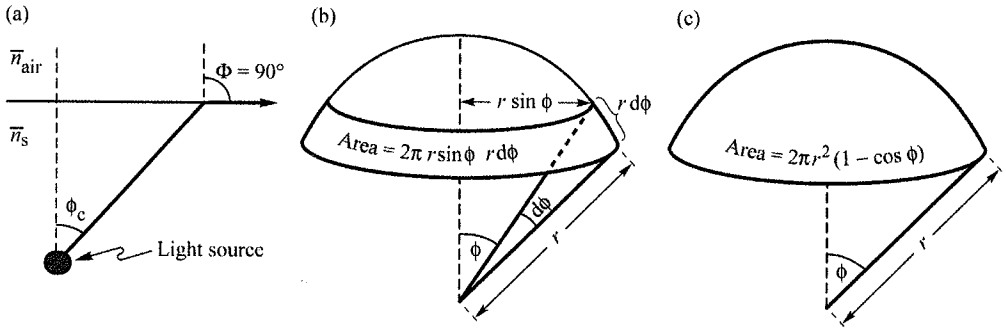

Fig. 5.3. (a) Definition of the escape cone by the critical angle ϕ_c. (b) Area element $\mathrm{d}A$. (c) Area of calotte-shaped section of the sphere defined by radius r and angle ϕ_c.

The calculation indicates that only a fraction of the light emitted inside a semiconductor can escape from the semiconductor. This fraction is given by

$$\boxed{\frac{P_{escape}}{P_{source}} = \frac{1}{2}(1 - \cos\phi_c)} \, . \tag{5.22}$$

Because the critical angle of total internal reflection for high-index materials is relatively small, the cosine term can be expanded into a power series. Neglecting higher-than-second-order terms yields

$$\frac{P_{\text{escape}}}{P_{\text{source}}} \approx \frac{1}{2}\left[1 - \left(1 - \frac{\phi_c^2}{2}\right)\right] = \frac{1}{4}\phi_c^2 . \tag{5.23}$$

Using the approximation of Eq. (5.19), one obtains

$$\boxed{\frac{P_{\text{escape}}}{P_{\text{source}}} \approx \frac{1}{4}\frac{\bar{n}_{\text{air}}^2}{\bar{n}_s^2}} . \tag{5.24}$$

The escape problem is a significant problem for high-efficiency LEDs. In most semiconductors, the refractive index is quite high (> 2.5) and thus only a small percentage of the light generated in the semiconductor can escape from a planar LED. The problem is less significant in semiconductors with a small refractive index and for polymers, which have refractive indices of the order of 1.5.

Exercise: ***Light escape from planar GaAs, GaN, and polymer LED structures.*** The refractive indices of GaAs, GaN, and light-emitting polymers are 3.4, 2.5, and 1.5, respectively. Calculate the critical angle of total internal reflection for GaAs, GaN, and for polymers. Also calculate the fraction of light power that can escape from a planar GaAs and GaN semiconductor structures and a polymer LED structure.

What improvement can be attained if a planar GaAs LED is encapsulated in a transparent polymer of refractive index 1.5, if the reflection at the polymer–air interface is neglected?

Solution:

Critical angle for total internal reflection:

GaAs $\phi_c = 17.1°$ GaN $\phi_c = 23.6°$ Polymer $\phi_c = 41.8°$.

Fraction of light that can escape:

GaAs 2.21% GaN 4.18% Polymer 12.7%.

Improvement of the GaAs planar LED due to polymer encapsulation: 232%.

5.4 Radiation pattern

All LEDs have a certain ***radiation pattern*** or ***far-field pattern***. The intensity, measured in W/cm^2, depends on the longitudinal and azimuth angle and the distance from the LED. The total optical power emitted by the LED is obtained by integration over the area of a sphere.

$$P = \int_A \int_\lambda I(\lambda)\, d\lambda\, dA \tag{5.25}$$

where $I(\lambda)$ is the ***spectral light intensity*** (measured in W per nm per cm^2) and A is the surface area of the sphere. The integration is carried out over the entire surface area.

5.5 The lambertian emission pattern

The index contrast between the light-emitting material and the surrounding material leads to a non-isotropic emission pattern. For high-index light-emitting materials with a planar surface, a lambertian emission pattern is obtained. Figure 5.4 illustrates a point-like light source located a short distance below a semiconductor–air interface. Consider a light ray emitted from the source at an angle ϕ with respect to the surface normal. The light ray is refracted at the semiconductor–air interface and the refracted light ray has an angle Φ with respect to the surface normal. The two angles are related by Snell's law, which, for small angles of ϕ (for which $\sin\phi \approx \phi$), can be written as

$$\bar{n}_s \, \phi \;=\; \bar{n}_{air} \sin\Phi \;. \tag{5.26}$$

Light emitted into the angle $d\phi$ in the semiconductor is emitted into the angle $d\Phi$ in air as shown in Fig. 5.4 (a). Differentiating the equation with respect to Φ and solving the resulting equation for $d\Phi$ yields

$$d\Phi \;=\; \frac{\bar{n}_s}{\bar{n}_{air}} \, \frac{1}{\cos\Phi} \, d\phi. \tag{5.27}$$

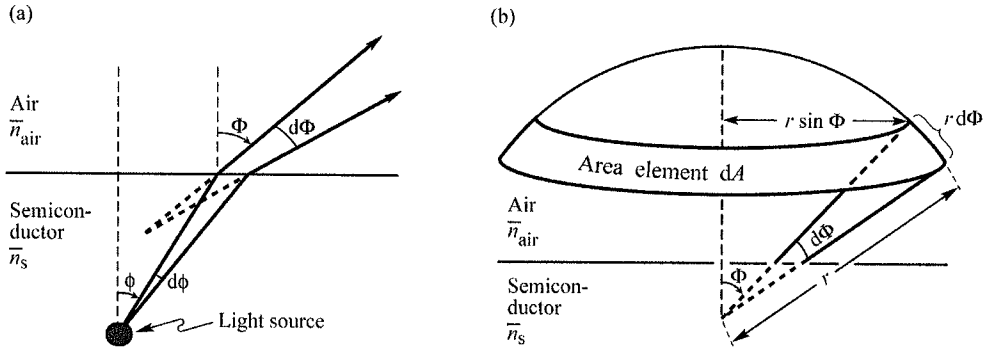

Fig. 5.4. Geometrical model used to derive the lambertian emission pattern. (a) The light emitted into angle $d\phi$ inside the semiconductor is emitted into the angle $d\Phi$ in air. (b) Illustration of the area element dA of the calotte-shaped section of the sphere.

Power conservation requires that the optical power emitted into the angle $d\phi$ in the semiconductor be equal to the optical power emitted into the angle $d\Phi$ in air, i.e.

$$I_s \, dA_s = I_{air} \, dA_{air} \tag{5.28}$$

where I_s and I_{air} are the light intensities (measured in units of W/m^2) in the semiconductor and air, respectively. Owing to the cylindrical symmetry of the emission pattern we choose the area element shown in Fig. 5.4 (b). The area element in air is given by

$$dA_{air} = 2\pi r \sin\Phi \, r \, d\Phi \, . \tag{5.29}$$

Using Eqs. (5.27) and (5.28) yields

$$dA_{air} = 2\pi r^2 \frac{\bar{n}_s^{\,2}}{\bar{n}_{air}^{\,2}} \frac{1}{\cos\Phi} \, \phi \, d\phi \, . \tag{5.30}$$

Similarly, the surface element in the semiconductor is given by

$$dA_s = 2\pi r \sin\phi \, r \, d\phi \approx 2\pi r^2 \, \phi \, d\phi \, . \tag{5.31}$$

The light intensity in the semiconductor at a distance r from the light source is given by the total source power divided by the surface area of a sphere with radius r, i.e.

$$I_s = \frac{P_{source}}{4\pi r^2} \, . \tag{5.32}$$

The light intensity in air can then be inferred from Eqs. (5.28), (5.30), (5.31), and (5.32). One obtains the ***lambertian emission pattern*** given by

$$\boxed{I_{air} = \frac{P_{source}}{4\pi r^2} \frac{\bar{n}_{air}^2}{\bar{n}_s^2} \cos\Phi} \, . \tag{5.33}$$

The lambertian emission pattern follows a cosine dependence on the angle Φ. The intensity is highest for emission normal to the semiconductor surface, i.e. for $\Phi = 0°$. At an angle of $\Phi = 60°$, the intensity decreases to half of its maximum value. The lambertian emission pattern is shown schematically in Fig. 5.5.

Several other surface shapes are also shown in Fig. 5.5. These non-planar surfaces exhibit various emission patterns. An isotropic emission pattern is obtained for hemispherically shaped LEDs, which have the light-emitting region in the center of the sphere. A strongly directed

emission pattern can be obtained in LEDs with parabolically shaped surfaces. However, both hemispherical as well as parabolic surfaces are difficult to fabricate.

The total power emitted into air can be calculated by integrating the intensity over the entire hemisphere. The total power is then given by

$$P_{\text{air}} = \int_{\Phi=0°}^{90°} I_{\text{air}} 2\pi r \sin\Phi \, r \, d\Phi \, . \tag{5.34}$$

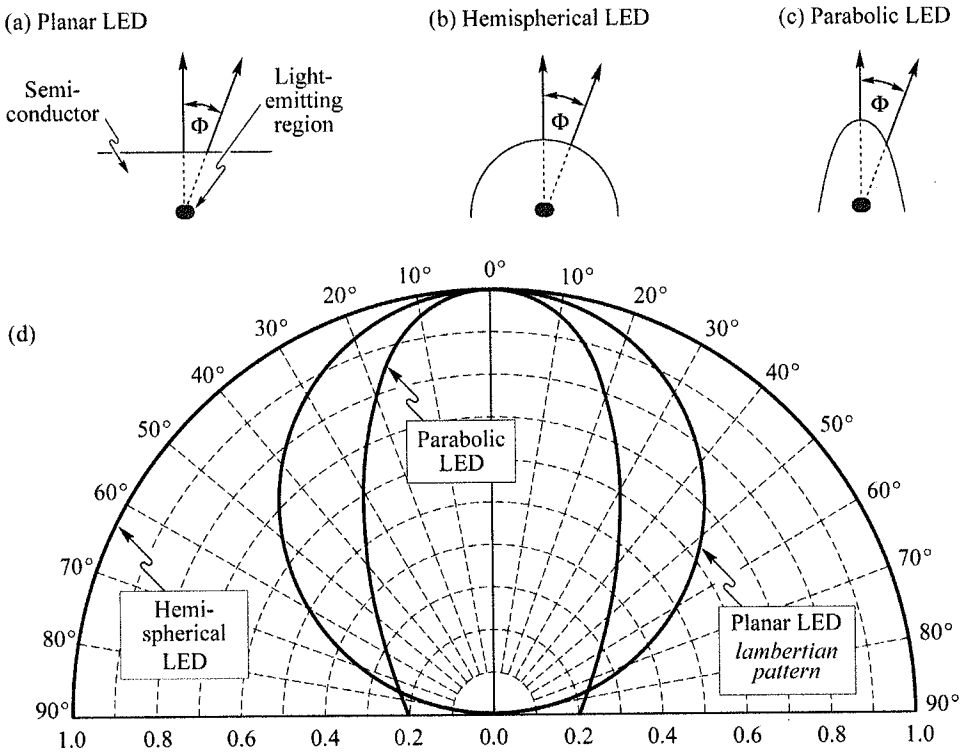

Fig. 5.5. Light-emitting diodes with (a) planar, (b) hemispherical, and (c) parabolic surfaces. (d) Far-field patterns of the different types of LEDs. At an angle of $\Phi = 60°$, the lambertian emission pattern decreases to 50% of its maximum value occurring at $\Phi = 0°$. The three emission patterns are normalized to unity intensity at $\Phi = 0°$.

By using the lambertian emission pattern for I_{air} in Eq. (5.34) and using $\cos\Phi \sin\Phi = (1/2) \sin(2\Phi)$, the integral can be calculated to yield

$$P_{\text{air}} = \frac{P_{\text{source}}}{4} \frac{\bar{n}_{\text{air}}^2}{\bar{n}_{\text{s}}^2} . \tag{5.35}$$

This result is identical to Eq. (5.24). This is not surprising because the light power that escapes from the semiconductor (P_{escape}) must be identical to the power in air (P_{air}).

In the calculation above, ***Fresnel reflection*** at the semiconductor–air interface has been neglected. At normal incidence, the Fresnel power transmittance is given by

$$T = 1 - R = 1 - \left(\frac{\bar{n}_{\text{s}} - \bar{n}_{\text{air}}}{\bar{n}_{\text{s}} + \bar{n}_{\text{air}}} \right)^2 = \frac{4\, \bar{n}_{\text{s}}\, \bar{n}_{\text{air}}}{(\bar{n}_{\text{s}} + \bar{n}_{\text{air}})^2} . \tag{5.36}$$

Fresnel reflection losses must be taken into account in a rigorous calculation.

Exercise: ***LED-to-fiber coupling efficiency.*** Consider a GaAs LED with a point-like light-emitting region located in close proximity to the planar GaAs LED surface. An optical fiber has an acceptance angle of 12° in air. What fraction of the light emitted by the active region can be coupled into the fiber? Assume a GaAs refractive index of 3.4. Neglect Fresnel reflection losses at the semiconductor–air and air–fiber interfaces.

Solution: The acceptance angle in the semiconductor is obtained from Snell's law and is 3.5°. Thus 0.093% of the power emitted by the active region can be coupled into the fiber.

5.6 Epoxy encapsulants

The light extraction efficiency can be enhanced by using dome-shaped encapsulants with a large refractive index. As a result of the encapsulation, the angle of total internal reflection through the top surface of the semiconductor is increased (Nuese *et al.*, 1969). It follows from Eq. (5.22) that the ratio of extraction efficiency with and without epoxy encapsulant is given by

$$\frac{\eta_{\text{epoxy}}}{\eta_{\text{air}}} = \frac{1 - \cos\phi_{\text{c,epoxy}}}{1 - \cos\phi_{\text{c,air}}} \tag{5.37}$$

where $\phi_{\text{c,epoxy}}$ and $\phi_{\text{c,air}}$ are the critical angles for total internal reflection at the semiconductor–epoxy and semiconductor–air interface, respectively. Figure 5.6 shows the calculated ratio of the extraction efficiency with and without an epoxy dome. Inspection of the figure yields that the efficiency of a typical semiconductor LED increases by a factor of 2–3 upon encapsulation with an epoxy having a refractive index of 1.5.

The inset of Fig. 5.6 shows that light is incident at an angle of approximately 90° at the

epoxy–air interface due to the dome-shape of the epoxy. Thus, total internal reflection losses do not occur at the epoxy–air interface. Besides improving the external efficiency of an LED, the encapsulant can also be used as a spherical lens for applications requiring a directed emission pattern. In polymer LEDs, encapsulants increase the extraction efficiency by only a small amount due to the inherently small refractive index of polymers.

Advanced encapsulants including graded-index encapsulants, encapsulants with a high refractive index ($\bar{n} > 2.0$), and encapsulants containing mineral diffusers will be discussed in the chapter on packaging.

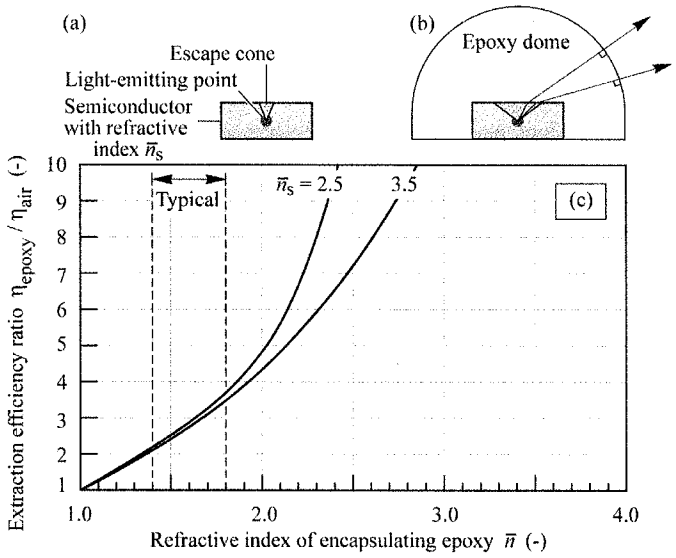

Fig. 5.6. LED (a) without and (b) with dome-shaped epoxy encapsulant. A larger escape angle is obtained for the LED with an epoxy dome. (c) Calculated ratio of light extraction efficiency emitted through the top surface of a planar LED with and without an epoxy dome. The refractive indices of typical epoxies range between 1.4 and 1.8 (adapted from Nuese *et al.*, 1969).

5.7 Temperature dependence of emission intensity

The emission intensity of LEDs decreases with increasing temperature. This decrease of the emission intensity is due to several temperature-dependent factors including (*i*) non-radiative recombination via deep levels, (*ii*) surface recombination, and (*iii*) carrier loss over heterostructure barriers.

Near room temperature, the temperature dependence of the LED emission intensity is frequently described by the phenomenological equation

$$I = I|_{300\,\mathrm{K}} \exp -\frac{T-300\,\mathrm{K}}{T_1} \tag{5.38}$$

where T_1 is the ***characteristic temperature***. A *high* characteristic temperature, implying a *weak* temperature dependence, is desirable.

It is interesting to note that both LEDs as well as semiconductor lasers have a distinct temperature dependence of the emission intensity. In LEDs, the decrease is expressed in terms of the "T_1 equation". In semiconductor lasers, the threshold current, i.e. the electrical current required for the onset of lasing, increases. In lasers the increase in threshold current is expressed in terms of the well-known T_0 equation. This equation is given by

$$I_{\mathrm{th}} = I_{\mathrm{th}}|_{300\,\mathrm{K}} \exp \frac{T-300\,\mathrm{K}}{T_0} \tag{5.39}$$

where I_{th} is the threshold current of the laser. Note the formal similarity of the "T_1 equation" (Eq. 5.38) and the "T_0 equation" (Eq. 5.39). Both equations are purely phenomenological equations intended to describe the experimental results without a strong theoretical framework allowing the derivation of the equations from basic principles.

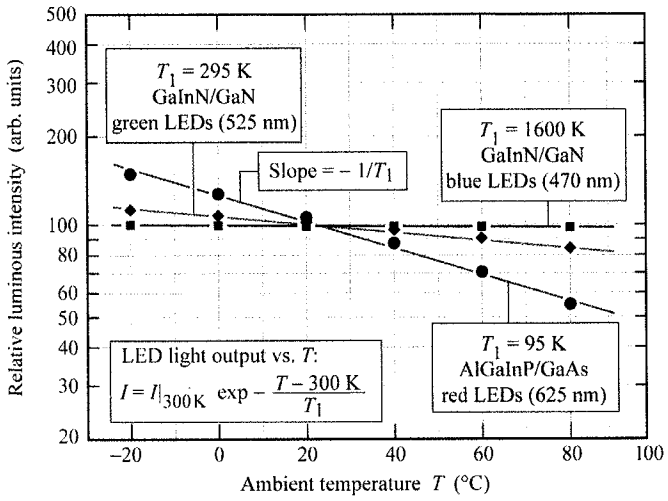

Fig. 5.7. Characteristic temperature T_1 of GaInN/GaN blue, GaInN/GaN green, and AlGaInP/GaAs red LEDs near room temperature (after data from Toyoda Gosei Corp., 2000). More recent data (Toyoda Gosei Corp., 2004) show the following values for T_1: Blue GaInN LED, 460 nm, T_1 = 1600 K; Cyan GaInN LED, 505 nm, T_1 = 832 K; Green GaInN LED, 525 nm, T_1 = 341 K; Red AlGaInP LED, 625 nm, T_1 = 199 K.

Experimental results of the temperature dependence of the emission intensity are shown in Fig. 5.7 (Toyoda Gosei Corporation, 2000). The figure shows the temperature dependence of the

emission intensity at a constant current for a blue GaInN/GaN, a green GaInN/GaN, and a red AlGaInP/GaAs LED. Inspection of Fig. 5.7 reveals that the blue LED has the highest T_1 and the red LED has the lowest T_1. III–V nitride LEDs have deeper wells so that carrier confinement is more effective in III–V nitride structures than in the III–V phosphide structures.

References

Nuese C. J., Tietjen J. J., Gannon J. J., and Gossenberger H. F. "Optimization of electroluminescent efficiencies for vapor-grown GaAsP diodes" *J. Electrochem Soc.: Solid State Sci.* **116**, 248 (1969)
Toyoda Gosei Corporation, Japan, General LED catalogue (2000)
Toyoda Gosei Corporation, Japan, General LED catalogue (2004)

11

Packaging

11.1 Low-power and high-power packages

Virtually all LEDs are mounted in a package that provides two electrical leads, a transparent optical window for the light to escape, and, in power packages, a thermal path for heat dissipation. The chip-encapsulating material advantageously possesses high optical transparency, a high refractive index, chemical inertness, high-temperature stability, and hermeticity. The refractive index contrast between the semiconductor and air is reduced by including an encapsulant thereby increasing the light extraction efficiency. Virtually all encapsulants are polymers with a typical refractive index of 1.5 to 1.8. A reduced index contrast at the semiconductor surface increases the angle of total internal reflection thereby enlarging the light escape cone and the extraction efficiency.

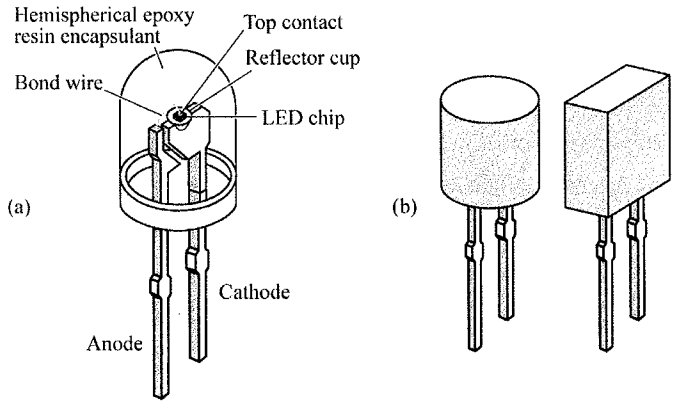

Fig. 11.1. Typical packages; (a) LED with hemispherical encapsulant; (b) LEDs with cylindrical and rectangular encapsulant.

A ***low-power package*** is shown in Fig. 11.1 (a). The active device is die-bonded or soldered to the bottom of a cup-like depression ("reflector cup") in one of the lead wires (usually the cathode lead). A bond wire connects the LED top contact to the other lead wire (usually the

anode lead). The LED package shown in the figure is frequently referred to as a "5 mm" or "T1-3/4" package.

In low-power LEDs, the encapsulant has the shape of a hemisphere, as shown in Fig. 11.1 (a), so that the angle of incidence at the encapsulant–air interface is always normal. As a result, total internal reflection does not occur at the encapsulant–air interface. There are types of LEDs that do *not* have a hemispherical shape for the encapsulant. Some LEDs have a rectangular or cylindrical shape with a planar front surface. Examples of such shapes are shown in Fig. 11.1 (b). Planar-surface LEDs are frequently used under circumstances where the intended viewing angle is close to normal incidence or where the LED is intended to blend in with a planar surface. Encapsulants provide protection against unwanted mechanical shock, humidity, and chemicals. The encapsulant also stabilizes the anode and cathode lead, the LED chip and bonding wire.

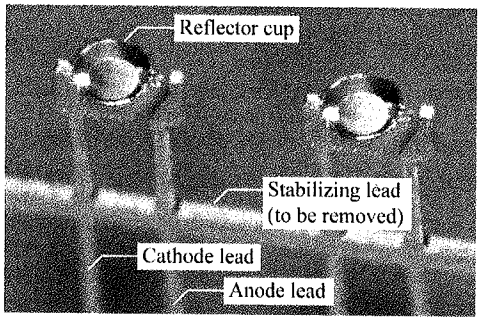

Fig. 11.2. Leadframe of a conventional 5 mm package for mounting and connecting LED chips. The stabilizing lead is cut off once mechanical stability between the anode and cathode lead has been established by the epoxy encapsulant.

A photograph of a series of LED ***leadframes*** is shown in Fig. 11.2. The individual leadframes are connected via a temporary stabilizing lead that is removed after die bonding, wire bonding, and the establishment of mechanical stability between anode and cathode lead by the epoxy encapsulant. The LED chip is die-bonded to the flat bottom of the highly reflective ***reflector cup*** with a silver-loaded electrically conductive epoxy being a common die-bonding material. Note that for power chips, metal-based solders are preferable as die-bonding materials due to their inherently lower thermal resistance compared with conductive epoxies.

A ***power package*** is shown in Fig. 11.3. Power packages have a *direct, thermally conductive path* from the LED chip, through the package, to a heat sink, e.g. a printed circuit board. The power package shown in the figure has several advanced features. Firstly, the package contains an Al or Cu heatsink slug with low thermal resistivity to which the LED submount is soldered by a metal-based solder. Secondly, the chip is encapsulated with silicone. Because standard silicone

retains mechanical softness in its cured state, the silicone encapsulant is covered with a plastic cover that also serves as lens. Thirdly, the chip is directly mounted on a Si submount that includes electrostatic discharge protection (ESD).

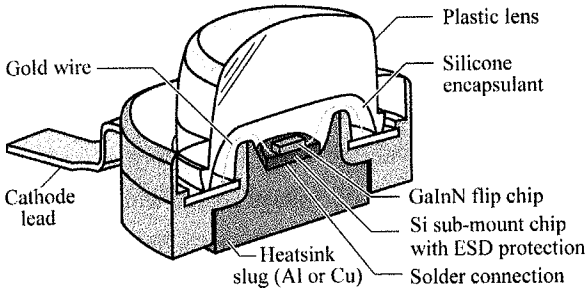

Fig. 11.3. Cross section through high-power package. The heatsink slug can be soldered to a printed circuit board for efficient heat removal. This package, called the *Barracuda package,* was introduced by Lumileds Corp. (adapted from Krames, 2003).

Photographs of the high-power package are shown in Fig. 11.4 including a high-magnification micrograph, Fig. 11.4 (b), revealing interdigitated contacts of a GaN-based LED. Fig. 11.4 (c) shows the package soldered to a printed-circuit board that possesses high thermal conductivity for efficient cooling (LED Museum, 2003). Several light-emitting diodes located on a single chip may be interconnected in series to increase operating voltage and decrease operating current of a device (Krames *et al.*, 2002, 2003).

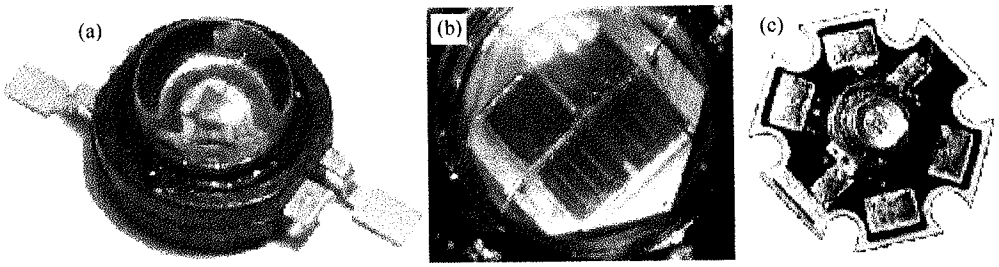

Fig. 11.4. (a) High-power package; (b) LED die in package; (c) package on printed circuit board with high thermal conductivity ((a) after Krames, 2003; (b), (c) after after LED Museum, 2003).

11.2 Protection against electrostatic discharge (ESD)

Electrostatic discharge (ESD) can be a major failure mechanism for electronic and optoelectronic components (Voldman, 2004). Consider that a charge $+Q$ is brought into contact with one of the diode electrodes. Consider further that the charge $+Q$ is discharged uniformly over a time Δt, so

that a current of $I = +Q/\Delta t$ flows through the device.

Let us first assume that the charge is brought into contact with the *cathode* of an LED and that the anode is grounded. The current will discharge with the diode in the reverse polarity. Taking the equivalent circuit of the reverse-biased diode as a capacitor C and a parallel resistor R_p, the voltage across the p-n junction in the steady state will rise to IR_p. Thus the energy dissipated in the device during the reverse discharge is then given by $I^2R_p\Delta t$.

Let us next assume that the charge is brought into contact with the *anode* of the LED and that the cathode is grounded. The current will discharge with the diode in the forward polarity. Taking the equivalent circuit of the forward-biased diode as a voltage source with voltage V_{th} with a series resistor R_s, the steady-state voltage across the p-n junction is $V_{th} + IR_s$, which, in the limit of a high current, can be approximated by IR_s. Thus the energy dissipated in the device during the forward discharge is approximately $I^2R_s\Delta t$.

Because $I^2R_p\Delta t >> I^2R_s\Delta t$, it is evident that the energy dissipated per reverse discharge event is much higher than the energy dissipated per forward discharge event, suggesting that *reverse* discharges are more damaging than *forward* discharges. This contention has indeed been confirmed by experiments (Wen *et al.*, 2004).

Wide-bandgap diodes (such as GaN-based diodes) are particularly prone to ESD failures, due to inherently high values of R_p (low reverse saturation currents and high breakdown voltages). This has spurred the development of ESD protection circuits for III–V nitride diodes (Steigerwald *et al.*, 2002; Sheu, 2003).

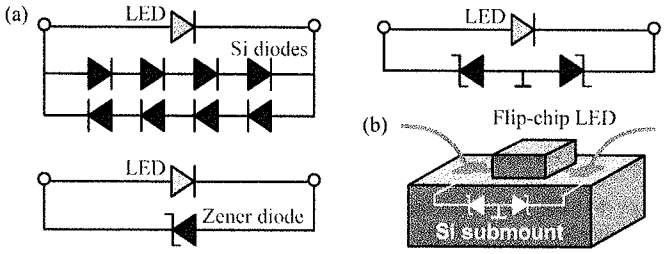

Fig. 11.5. (a) Electrostatic discharge (ESD) protection circuits using multiple Si p-n junctions, one Zener diode, and two Zener diodes. (b) ESD protection integrated into a Si submount (two-Zener diode circuit after Lumileds, 2004).

Electrostatic discharge-protection circuits can consist of a series of Si diodes, one Si Zener diode, or two Si Zener diodes, as shown in Fig. 11.5, with two Zener diodes being a common configuration (Steigerwald *et al.*, 2002; Lumileds, 2004). The current caused by an electrostatic discharge will bypass the LED and flow through the ESD protection circuit, particularly for reverse discharges. ESD protection circuits have been integrated with Si submounts (Steigerwald

et al., 2002; Lumileds, 2004). Using one or two Zener diodes or placing several Si diodes in series increases the threshold voltage of the ESD circuit to values beyond the turn-on voltage of the LED. Thus, under normal operating conditions, the current through the ESD circuit is negligibly small.

Sheu (2003) proposed a Schottky diode integrated with the LED on the same chip. The structure, shown in Fig. 11.6 (a), consists of a large-area p-n junction diode and, separated by a deep trench, a small-area Schottky diode. The Schottky diode, fabricated on the n-type buffer layer of a GaInN LED, is forward biased when the LED is biased in the reverse polarity. For reverse electrostatic discharges, the current flows mostly through the Schottky diode, thereby bypassing the p-n junction and preventing damage to the p-n junction. For forward electrostatic discharges, the current flows through the p-n junction. In an alternative structure, shown in Fig. 11.6 (b), the Schottky diode is replaced by a p-n junction diode (Cho, 2005).

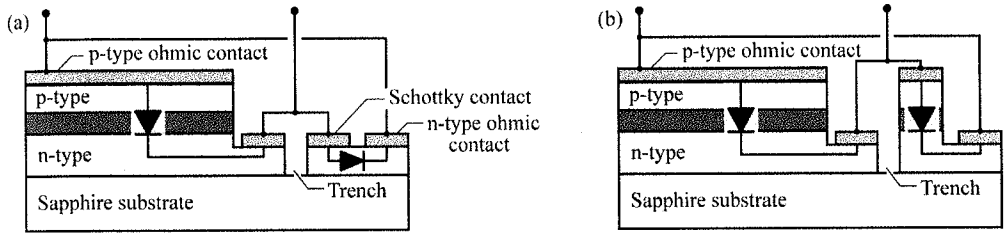

Fig. 11.6. On-chip ESD protection using (a) a small-area Schottky diode on the n-type buffer layer of a GaInN device and (b) a small-area p-n junction diode (Schottky diode circuit after Sheu, 2003).

11.3 Thermal resistance of packages

The thermal resistance of LED packages together with the maximum temperature of operation determines the maximum thermal power that can be dissipated in the package. The maximum temperature of operation may be determined by reliability considerations, by the degradation of the encapsulant, and by internal-quantum-efficiency considerations. Several types of LED packages and their thermal resistance are shown in Fig. 11.7 (Arik *et al.*, 2002). Early LED packages, introduced in the late 1960s and still used for low-power packages at the present time, have a high thermal resistance of about 250 K/W. Packages using ***heatsink slugs*** made of Al or Cu that transfer heat from the chip directly to a printed circuit board (PCB), which in turn spreads the heat, have thermal resistances of 6–12 K/W. It is expected that thermal resistances of

< 5 K/W will be achieved for advanced passively cooled power packages.

Note that the packages shown in Fig. 11.7 do not use ***active cooling***, i.e. fan cooling. Heatsinks with cooling fins and fan are commonly used to cool electronic microchips including Si CMOS microprocessors. They have thermal resistances < 0.5 K/W. The use of active cooling devices would reduce the power efficiency of LED-based lighting systems.

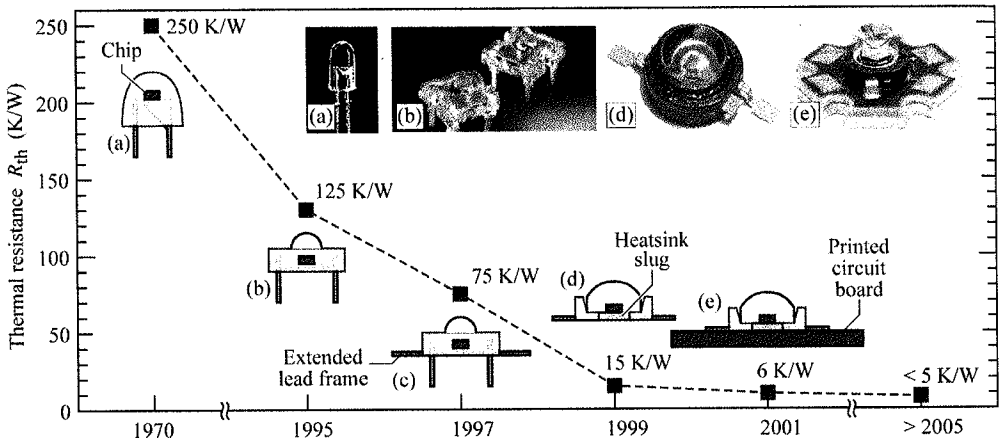

Fig. 11.7. Thermal resistance of LED packages: (a) 5mm (b) low-profile (c) low-profile with extended lead frame (d) heatsink slug (e) heatsink slug mounted on printed circuit board (PCB). Trade names for these packages are "Piranha" (b and c, Hewlett Packard Corp.), "Barracuda" (d and e, Lumileds Corp.), and "Dragon" (d and e, Osram Opto Semiconductors Corp.) (adapted from Arik *et al.*, 2002).

11.4 Chemistry of encapsulants

Encapsulants have several requirements including high transparency, high refractive index, chemical stability, high-temperature stability, and hermeticity. All encapsulants are based on polymers, several of which are shown in Fig. 11.8. A simple polymer molecule consisting of a hydrocarbon chain is shown in Fig. 11.8 (a). Branching and cross linking the polymer molecule results in rubber compounds as shown in Fig. 11.8 (b). Such rubber compounds lack transparency and cannot be used as LED encapsulants. However, it is well known that oxides are frequently transparent. In fact, all encapsulants used for LEDs contain oxygen.

A common encapsulant is ***epoxy resin*** (also called epoxy), which remains transparent and does not show degradation over many years for long-wavelength visible-spectrum and IR LEDs. However, it has been reported that epoxy resins lose transparency in LEDs emitting at shorter

wavelengths, i.e. in the blue, violet, and UV (Barton *et al.*, 1998). Epoxy resins are chemically stable up to temperatures of about 120 °C. Prolonged exposure to temperatures greater than 120 °C leads to yellowing (loss of transparency).

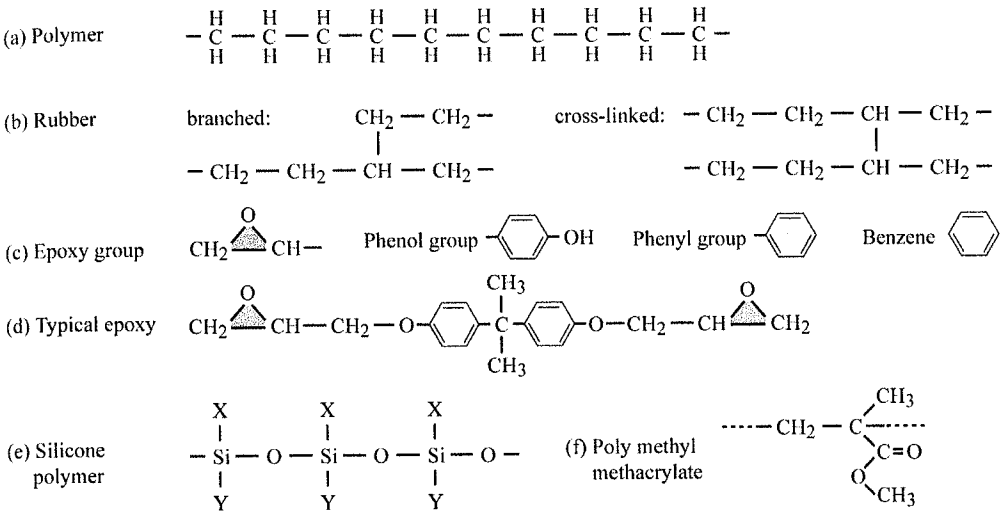

Fig. 11.8. Chemical structures of polymers. Epoxy resins, silicone polymers, and poly methyl methacrylate (PMMA) are used as LED encapsulants. In the silicone structure, X and Y represent atoms or molecules such as H, CH_3 (methyl), C_6H_5 (phenyl).

The ***epoxy group*** shown in Fig. 11.8 (c) contains an O atom attached to two C atoms already bonded to each other. Such a three-membered ring consisting of one oxygen and two carbon atoms is part of the epoxy resin structure shown in Fig. 11.8 (d). Solid epoxy resins are formed by stoichiometrically mixing two liquid compounds, an epoxide with another compound, a resin, having two hydroxyl groups. ***Resins*** are oil-like substances that frequently have phenol groups. The phenol group, $-C_6H_4-OH$, is derived from the phenyl group, $-C_6H_5$ by removing one H atom and replacing it with the hydroxyl group, –OH. The phenyl group is derived from benzene, the well-known six-atom carbon ring, C_6H_6, by removing one H atom. Under a thermal-setting process, the epoxide groups co-polymerize with hydroxyl groups of the resin.

Typical epoxy resins for encapsulation are thermally curable two-part liquid systems consisting of bisphenol-A based or cycloaliphatic epoxide and anhydride (Kumar *et al.*, 2001). The formation of the epoxy resin requires a short high-temperature cure (120 °C). The two-part system has to be in stoichiometric proportions. Resin-rich compositions lead to lower glass transition temperatures while hardener-rich compositions may lead to discoloration of the

encapsulant. The refractive index of epoxy resin is near 1.6. Besides being transparent, epoxy resin is noted for its good mechanical properties and good thermal stability. However, prolonged exposure of the epoxy to temperatures exceeding 120 °C will lead to discoloration and loss of transparency. In addition to thermo-setting epoxy resins, UV-curable and microwave-curable epoxy resins have been reported (Kumar *et al.* 2001; Gorczyk, 2001; Flick, 1993).

To overcome the limited thermal stability of epoxies, ***silicone encapsulants*** have been used since the early 2000s. Silicone is thermally stable up to temperatures of about 190 °C, significantly higher than epoxies (Crivello, 2004). Furthermore silicone is flexible (and remains flexible for decades) thereby reducing the mechanical stress on the semiconductor chip. ***Silicone*** is a polymer whose basic structure is shown in Fig. 11.8 (e). Silicone contains Si and O thereby resembling SiO_2 more so than epoxy resins. This resemblance suggests that silicone encapsulants are chemically and thermally stable and do not lose transparency as easily as epoxy resins. It may be desirable to develop encapsulants that are SiO_2-like because SiO_2 has excellent thermal and chemical stability and very high transparency (Crivello, 2004). On the other hand, silica lacks the flexibility that silicones offer.

Poly methyl methacrylate or briefly ***PMMA*** is a less common encapsulant used for LEDs. The chemical structure of methyl methacrylate, the elementary cell of PMMA, is shown in Fig. 11.8 (f). PMMA is also known under the name of acrylic glass and under the product name Plexiglas. The relatively low refractive index of PMMA ($\overline{n}$ = 1.49 in the wavelength range 500–650 nm) results in a limited extraction efficiency when used with high-index semiconductors.

11.5 Advanced encapsulant structures

Graded-index encapsulants consisting of several layers with different refractive indices were demonstrated by Lee *et al.* (2004). The layer of highest refractive index is in contact with the semiconductor chip. The outer layers of the encapsulant have lower refractive indices. Extraction efficiencies exceeding those with a constant refractive index can be attained by using such refractive-index graded encapsulants.

Encapsulants containing ***mineral diffusers*** cause light to reflect, refract, and scatter, thereby randomizing the propagation direction and isotropizing the far-field distribution. For multi-color devices (e.g. multi-chip white LEDs), mineral diffusers uniformize the color distribution. Mineral diffusers are optically transparent substances, such as TiO_2, CaF_2, SiO_2, $CaCO_3$, and $BaSO_4$, with a refractive index different from that of the encapsulant (Reeh *et al.*, 2003).

Encapsulants containing ***nanoparticles*** with a high refractive index (e.g. titania, magnesia,

yttria, zirconia, alumina, GaN, AlN, ZnO, ZnSe) have been proposed by Lester *et al.* (1998). Nanoparticles embedded into a host (usually a polymer) do not scatter light if they are uniformly distributed and if their size is much smaller than the wavelength. The refractive index of the of the nanoparticle-loaded encapsulant is given by

$$\bar{n} = \frac{\bar{n}_{\text{host}} V_{\text{host}} + \bar{n}_{\text{nano}} V_{\text{nano}}}{V_{\text{host}} + V_{\text{nano}}} \tag{11.1}$$

where V_{host} and V_{nano} refer to the volume of the host and nanoparticles, respectively. For high loading factors, the refractive index of the encapsulant can significantly exceed that of the host, thereby enlarging the semiconductor escape cone and increasing the extraction efficiency.

References

Arik M., Petroski J., and Weaver S. "Thermal challenges in the future generation solid state lighting applications: light emitting diodes" *Eighth Intersociety Conference on Thermal and Thermomechanical Phenomena in Electronic Systems* (Cat. No.02CH37258) May 30–June 1 2002, p. 113 (IEEE, Piscataway NJ, 2002)

Barton D. L., Osinski M., Perlin P., Helms C. J., and Berg N. H. "Life tests and failure mechanisms of GaN/AlGaN/InGaN light-emitting diodes" *Proc. SPIE* **3279**, 17 (1998)

Cho J., Samsung Advanced Institute of Technology, Suwon, Korea, personal communication (2005)

Crivello J. V., Rensselaer Polytechnic Institute, personal communication (2004)

Flick E. W. *Epoxy Resins, Curing Agents, Compounds, and Modifiers: An Industrial Guide* (Noyes Data Corporation/Noyes Publications, Park Ridge NJ, 1993)

Gorczyk J., Bogdal D., Pielichowski J., and Penczek P. "Synthesis of high molecular weight epoxy resins under microwave irradiation" *Fifth International Electronic Conference on Synthetic Organic Chemistry* (ECSOC-5), http://www.mdpi.org/ecsoc-5.htm, 1–30 (September 2001)

Krames M. R., Steigerwald D. A., Kish Jr. F. A., Rajkomar P., Wierer Jr. J. J., and Tan T. S. "III-nitride light-emitting device with increased light generating capability" US Patent 6,486,499 B1 (2002)

Krames M. R. "Overview of current status and recent progress of LED technology" *US Department of Energy Workshop "Solid State Lighting – Illuminating the Challenges"* Crystal City, VA, Nov. 13–14, 2003

Kumar R. N., Keem L. Y., Mang N. C., and Abubakar A. "Ultraviolet radiation curable epoxy resin encapsulant for light-emiting diodes" *4th International Conference on Mid-Infrared Optoelectronics Materials and Devices* (MIOMD) (2001)

LED Museum, http://ledmuseum.home.att.net/agilent.htm (2003)

Lee B. K., Goh K. S., Chin Y. L., and Tan C. W. "Light emitting diode with gradient index layering" US Patent 6,717,362 B1 (2004)

Lester S. D., Miller J. N., and Roitman D. B. "High refractive index package material and light emitting device encapsulated with such material" US Patent 5,777,433 (1998)

Lumileds Corporation *Luxeon reliability* Application Brief **AB25**, 11 (2004)

Reeh U., Höhn K., Stath N., Waitl G., Schlotter P., Schneider J., and Schmidt R. "Light-radiating semiconductor component with luminescence conversion element" US Patent 6,576,930 B2 (2003)

Sheu J.-K. "Group III–V element-based LED having ESD protection capacity" US Patent 6,593,597 B2 (2003)

Steigerwald D. A., Bhat J. C., Collins D., Fletcher R. M., Holcomb M. O., Ludowise M. J., Martin P. S., and Rudaz S. L. "Illumination with solid state lighting technology" *IEEE J. Sel. Top. Quantum Electron.* **8**, 310 (2002)

Voldman S. H. *ESD: Physics and Devices* (John Wiley and Sons, New York, 2004)
Wen T. C., Chang S. J., Lee C. T., Lai W. C., and Sheu J. K. "Nitride-based LEDs with modulation-doped AlGaN-GaN superlattice structures" *IEEE Trans. Electron Dev.* **51**, 1743 (2004)

15

Resonant-cavity light-emitting diodes

15.1 Introduction and history

The resonant-cavity light-emitting diode (RCLED) is a light-emitting diode that has a light-emitting region inside an optical cavity. The optical cavity has a thickness of typically one-half or one times the wavelength of the light emitted by the LED, i.e. a fraction of a micrometer for devices emitting in the visible or in the infrared. The resonance wavelength of the cavity coincides or is in resonance with the emission wavelength of the light-emitting active region of the LED. Thus the cavity is a *resonant cavity*. The spontaneous emission properties from a light-emitting region located inside the resonant cavity are enhanced by the resonant-cavity effect. The RCLED is the first practical device making use of spontaneous emission enhancement occurring in microcavities.

The placement of an active region inside a resonant cavity results in multiple improvements of the device characteristics. Firstly, the light intensity emitted from the RCLED along the axis of the cavity, i.e. normal to the semiconductor surface, is higher compared with conventional LEDs. The enhancement factor is typically a factor of 2–10. Secondly, the emission spectrum of the RCLED has a *higher spectral purity* compared with conventional LEDs. In conventional LEDs, the spectral emission linewidth is determined by the thermal energy kT. However, in RCLEDs, the emission linewidth is determined by the quality factor (Q factor) of the optical cavity. As a result, the spectral emission width of the RCLED is a factor of 2–5 narrower compared with conventional LEDs. For the same reason, the wavelength shift with temperature is determined by the temperature coefficient of the optical cavity and not by the energy gap of the active material. This results in a significantly higher temperature stability of the RCLED emission wavelength compared with conventional LEDs. Thirdly, the emission far-field pattern of the RCLED is more *directed* compared with conventional LEDs. In conventional LEDs, the emission pattern is lambertian (i.e. cosine-function-like). In an RCLED, the emission pattern is directed mostly along the optical axis of the cavity.

These characteristics of RCLEDs are desirable for local-area, medium bit rate optical communication systems. LEDs play an important role in local-area (< 5 km) medium bit rate (< 1 Gbit/s) optical communication networks. In particular, plastic optical fibers are increasingly used for optical communication over short distances. The higher emission intensity and the more directed emission pattern afforded by the RCLED increase the power coupled into the optical fiber. As a result, the RCLED can transmit data over longer distances. Furthermore, the higher spectral purity of RCLEDs results in less chromatic dispersion allowing for higher bit rates.

Light-emitting diodes are the transmitter device of choice for medium bit rate optical communication over distances less than 5 km. Compared with lasers, LEDs are less expensive, more reliable, and less temperature sensitive. The RCLED has improved characteristics compared with conventional LEDs while maintaining the inherent advantages of LEDs. The reflectivity of the RCLED reflectors is lower compared with vertical-cavity surface-emitting lasers (VCSELs), thereby allowing for a lower RCLED manufacturing cost compared with VCSELs. At 650 nm, the preferred communication wavelength for plastic optical fibers, VCSELs are difficult to manufacture due to the lack of high-reflectivity reflectors.

RCLEDs are also used for high-brightness applications (Streubel *et al.*, 1998; Wirth *et al.*, 2001, 2002). In these devices, the resonance wavelength is designed to be at the long-wavelength end of the spontaneous emission spectrum of the semiconductor. This ensures that the emission intensity, integrated over all spatial directions, is maximized.

The enhanced spontaneous emission occurring in resonant-cavity structures can be beneficially employed in semiconductor and polymer LEDs. Resonant-cavity light-emitting diodes were first realized in 1992 (Schubert *et al.*, 1992a) in the GaAs material system. About a year later, RCLEDs were demonstrated in organic materials (Nakayama *et al.*, 1993).

Resonant-cavity structures with enhanced spontaneous emission also include Er-doped microcavities (Schubert *et al.*, 1992b). Owing to the inherently narrow luminescence line of intra-atomic Er radiative transitions, there is a very good overlap between the cavity optical mode and the Er luminescence line. At the present time, no Er-doped current-injection devices exist. However, the great potential of Er-doped resonant cavities makes the realization of Er-doped RCLEDs likely in the future.

15.2 RCLED design rules

The basic structure of an RCLED is shown in Fig. 15.1 and comprises two mirrors with reflectivity R_1 and R_2. The reflectivity of the two mirrors is chosen to be unequal so that the light

exits the cavity predominantly through one of the mirrors. This mirror is called the ***light-exit mirror***. Here we designate the mirror with reflectivity R_1 as the light-exit mirror. An active region is located between the mirrors, preferably at the antinode location of the standing optical wave of the cavity, as shown in Fig. 15.1. Metal mirrors are assumed in Fig. 15.1 so that the wave amplitude is zero at the location of the mirrors.

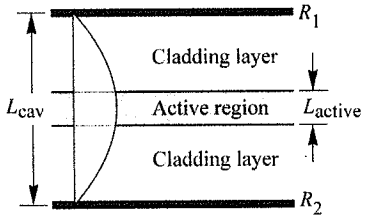

Fig. 15.1. Schematic illustration of a resonant cavity consisting of two metal mirrors with reflectivity R_1 and R_2. The active region has a thickness L_{active} and an absorption coefficient α. Also shown is the standing optical wave. The cavity length L_{cav} is equal to $\lambda/2$.

Next, we summarize several design rules intended to maximize the spontaneous emission enhancement in resonant-cavity structures (Schubert *et al.*, 1994, 1996; Hunt *et al.*, 1995a, 1995b). These rules will provide further insight into the fundamental operating principles of RCLEDs and the differences of these devices with respect to VCSELs.

The ***first design criterion*** for RCLEDs is that the reflectivity of the light-exit reflector, R_1, should be much lower than the reflectivity of the back reflector, i.e.

$$R_1 \ll R_2 \,. \tag{15.1}$$

This condition ensures that light exits the device mainly through the reflector with reflectivity R_1. Equation (15.1) applies to the design of communication RCLEDs, where light is emitted into the small core of a multimode fiber, and display RCLEDs, where light should be emitted towards the observer.

The ***second design criterion*** calls for the shortest possible cavity length L_{cav}. In order to derive this criterion, the integrated enhancement, discussed in a preceding section, can be rewritten by using the expressions for the cavity finesse F and cavity quality factor Q. One obtains

$$G_{int} = \frac{\xi}{2}\frac{2}{\pi}\frac{1-R_1}{1-\sqrt{R_1R_2}}\sqrt{\pi \ln 2}\,\frac{\lambda}{\Delta\lambda_n}\frac{\lambda_{cav}}{L_{cav}}\frac{\tau_{cav}}{\tau} \tag{15.2}$$

where λ and λ_{cav} are the active region emission wavelengths in vacuum and inside the cavity,

respectively. Since the emission wavelength λ and the natural linewidth of the active medium, $\Delta\lambda_n$, are given quantities, Eq. (15.2) shows that minimization of the cavity length L_{cav} maximizes the integrated intensity.

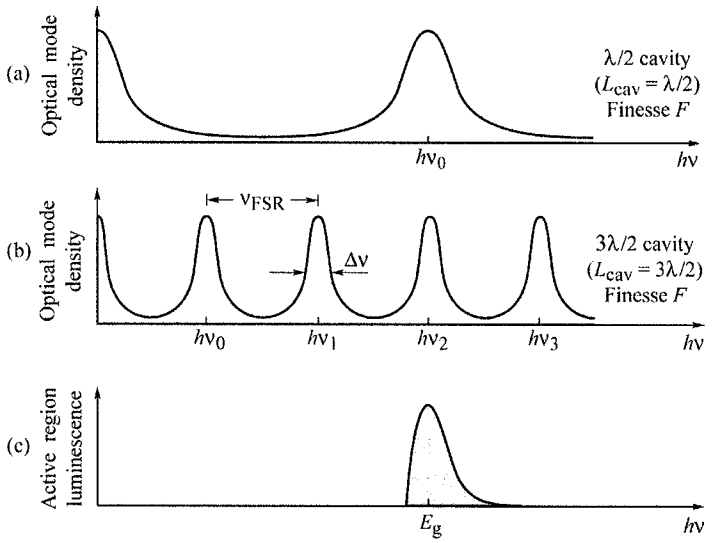

Fig. 15.2. Optical mode density for (a) a short and (b) a long cavity with the same finesse F. (c) Spontaneous free-space emission spectrum of an LED active region. The spontaneous emission spectrum has a better overlap with the short-cavity mode spectrum compared with the long-cavity mode spectrum.

The importance of a short cavity length is elucidated by Fig. 15.2. The optical mode densities of two different cavities, namely a short and a long cavity, are shown in Figs. 15.2 (a) and (b), respectively. Both cavities have the same mirror reflectivities and finesse. The natural emission spectrum of the active region is shown in Fig. 15.2 (c). The best overlap between the resonant optical mode and the active region emission spectrum is obtained for the shortest cavity.

The largest enhancements are achieved with the shortest cavities, which in turn are obtained if the *fundamental* cavity mode is in resonance with the emission from the active medium. The cavity length is also reduced by using a DBR with a short penetration depth, i.e. a DBR consisting of two materials with a large difference in the refractive index.

The ***third design criterion*** is the minimization of self-absorption in the active region. This criterion can be stated as follows: the reabsorption probability of photons emitted from the active region into the cavity mode should be much smaller than the escape probability of photons through one of the reflectors. Assuming $R_2 \approx 1$, this criterion can be written as

$$2\xi\alpha L_{active} < (1-R_1) \tag{15.3}$$

where α and L_{active} are the absorption coefficient and the thickness of the active region, respectively. If the criterion of Eq. (15.3) were not fulfilled, photons would most likely be reabsorbed by the active region. Subsequently, re-emission will, with a certain probability, occur along the lateral direction (waveguided modes), i.e. not into the cavity mode. Another possibility is that the electron–hole pairs generated by reabsorption recombine non-radiatively. In either case, reabsorption processes occurring in high-finesse cavities *reduce the cavity mode emission out of the cavity*. Thus, if the condition of Eq. (15.3) is not fulfilled, the emission intensity of resonant cavities is lowered rather than enhanced.

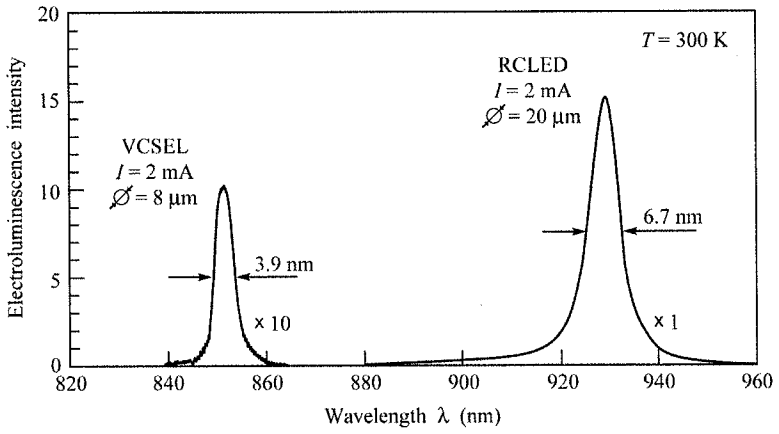

Fig. 15.3. Spontaneous electroluminescence spectrum of a vertical-cavity surface-emitting laser (VCSEL) emitting at 850 nm and of a resonant-cavity light-emitting diode (RCLED) emitting at 930 nm. The drive current for both devices is 2 mA. The VCSEL spectrum is multiplied by a factor of 10. The threshold current of the VCSEL is 7 mA (after Schubert *et al.*, 1996).

Whereas the condition of Eq. (15.3) is fulfilled in RCLEDs, it is clearly not fulfilled in VCSELs. The spontaneous emission intensities of RCLEDs and VCSELs were compared by Schubert *et al.* (1996). In this comparison, the VCSEL and the RCLED were driven by an injection current of 2 mA, which is below the threshold current of the VCSEL of $I_{th} = 7$ mA. The spontaneous emission spectra of an RCLED and a VCSEL are shown in Fig. 15.3. The VCSEL has an AlGaAs/GaAs quantum well active region emitting at 850 nm. Both reflectors of the VCSEL are AlGaAs/AlAs DBRs. Figure 15.3 reveals that the emission intensity of the VCSEL in the *spontaneous* regime is more than a factor of 15 lower than the emission intensity from the RCLED.

Because the magnitude of the maximum gain in semiconductors is always lower than the

magnitude of the absorption coefficient in an unpumped semiconductor ($|g| < |\alpha|$), VCSELs could not lase if the condition of Eq. (15.3) were met. Thus, the spontaneous emission intensity in VCSELs is low and *must be low* in order to enable the device to lase. Figure 15.3 also reveals that the emission spectral linewidth of VCSELs is narrower than that of RCLEDs. The higher spectral purity is due to the higher values of R_1 and R_2 as required for VCSELs.

The fulfillment of Eq. (15.3) by RCLEDs also implies that these devices *cannot lase*. As stated above, it is always $|g| < |\alpha|$. Consequently, the mirror loss $(1 - R_1)$ is always larger than the maximum achievable round-trip gain $(2\xi g L_{active})$. The fundamental inability of RCLEDs to lase has been verified experimentally by pulsed injecting currents of large magnitude without finding any evidence for lasing. These considerations show that the device physics of RCLEDs and VCSELs is fundamentally different.

The arguments used above imply that the *spontaneous* emission into the fundamental cavity mode in VCSEL structures is very low due to reabsorption of photons by the active region. A reduction of the threshold current by increasing the reflectivity will be accompanied by a further decrease of the *spontaneous* emission below threshold. We therefore conclude that the so-called zero-threshold laser (Kobayashi *et al.* 1982; Yokoyama, 1992) cannot be realized by a planar resonant-cavity structure.

15.3 GaInAs/GaAs RCLEDs emitting at 930 nm

The structure of an RCLED with a GaInAs active region is shown in Fig. 15.4 (a). The cavity is defined by one distributed Bragg reflector (DBR) and one metallic reflector. Also included are two confinement regions and a four-quantum-well active region. The heavily doped n-type substrate is coated with a ZrO_2 anti-reflection layer (Schubert *et al.*, 1994). A picture of the first RCLED is shown in Fig. 15.4 (b).

The motivation for the metal reflector is twofold. Firstly, the metallic Ag reflector serves as a non-alloyed ohmic contact to the heavily doped p-type ($N_A \approx 5 \times 10^{19}$ cm^{-3}) GaAs top layer, thus effectively confining the pumped region to the area below the contact. Secondly, it was shown in the preceding section that the cavity length must be kept as short as possible for maximizing the emission enhancement. Owing to the lack of a penetration depth, metal reflectors allow for a short cavity length. Cavities with two metallic reflectors have been reported (Wilkinson *et al.*, 1995). However, optical absorption losses in the light-exit mirror can be large in a double metal mirror structure, unless very thin metallic reflectors are used (Tu *et al.*, 1990). The lack of a p-type DBR also avoids the well-known problem of high resistance in p-type DBRs (Schubert *et*

al., 1992c; Lear and Schneider, 1996). It has been shown that parabolic grading yields the lowest ohmic resistance in DBRs. Such parabolic grading is suited to eliminating heterojunction band discontinuities (Schubert *et al.*, 1992c).

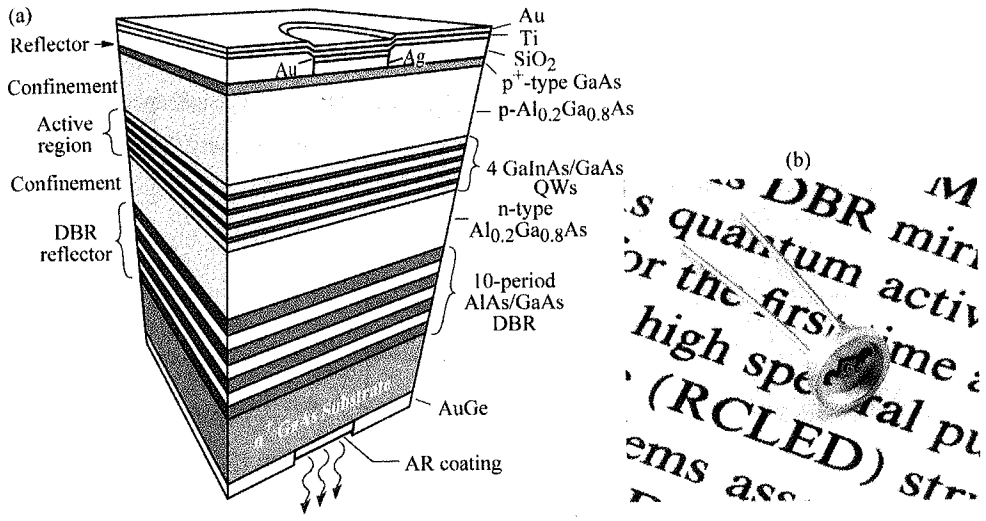

Fig. 15.4. (a) Schematic structure of a substrate-emitting GaInAs/GaAs RCLED consisting of a metal top reflector and a bottom distributed Bragg reflector (DBR). The RCLED emits at 930 nm. The reflectors are an AlAs/GaAs DBR and a Ag top reflector. (b) Picture of the first RCLED (after Schubert *et al.*, 1994).

The magnitude of the reflectivity of the DBR needs to be consistent with Eqs. (15.1) and (15.3). The Ag back mirror has a reflectivity of approximately 96%. According to Eq. (15.1), the DBR reflectivity must be $< 96\%$. The second criterion of Eq. (15.3) requires that $2\xi\alpha L_{\text{active}} < 1 - R_1$. Assuming $\xi = 1.3$, $\alpha = 10^4$ cm^{-1}, $L_{\text{active}} = 400$ Å, one obtains the condition $R_1 < 90\%$. Thus the mirror reflectivity of RCLEDs must be much lower than that of VCSELs. A high reflectivity would increase self-absorption and decrease the light output of the device as discussed earlier. De Neve *et al.* (1995) used an extensive theoretical model to calculate the mirror reflectivity. The maximum efficiency was calculated at a reflectivity of $R_1 = 50$–60%.

The reflection and emission properties of the RCLED are shown in Figs. 15.5 (a) and (b). The reflection spectrum of the RCLED (Fig. 15.5 (a)) exhibits a highly reflective band for wavelengths > 900 nm and a dip in the reflectivity at the cavity resonance. The spectral width of the cavity resonance is 6.3 nm. The emission spectrum of an electrically pumped device, shown in Fig. 15.5 (b), has nearly the same shape and width as the cavity resonance.

In conventional LEDs, the spectral characteristics of the devices reflect the thermal distribution of electrons and holes in the conduction and valence bands. The spectral characteristics of light emission from microcavities are as intriguing as they are complex. However, restricting our considerations to the optical axis of the cavity simplifies the cavity physics considerably. If we assume that the cavity resonance is much narrower than the natural emission spectrum of the semiconductor, then the on-resonance luminescence is enhanced whereas the off-resonance luminescence is suppressed. The on-axis emission spectrum should therefore reflect the enhancement, that is, the resonance spectrum of the cavity. The experimental results shown in Fig. 15.5 confirm this conjecture.

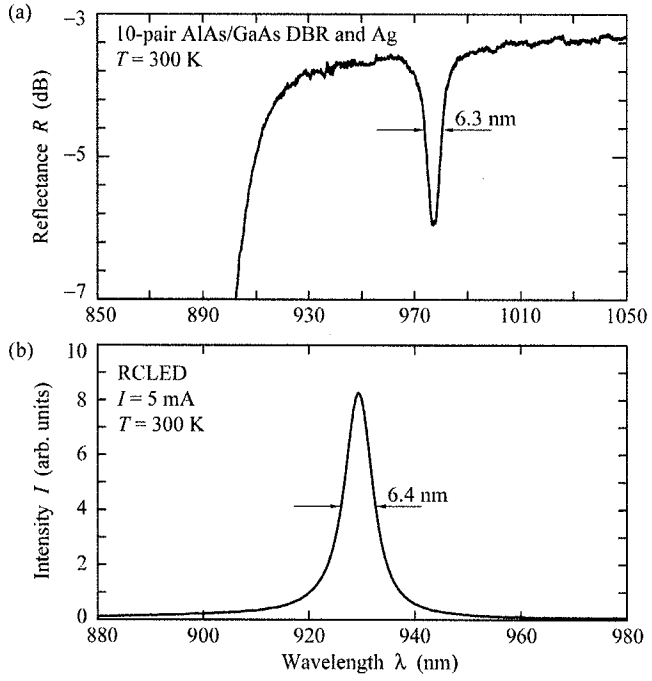

Fig. 15.5. (a) Reflectance of a resonant cavity consisting of a 10-pair AlAs/GaAs distributed Bragg reflector and an Ag reflector. (b) Emission spectrum of an RCLED consisting of a 10-pair AlAs/GaAs distributed Bragg reflector and an Ag reflector (after Schubert *et al.*, 1994).

Owing to the cavity, the emission spectrum of an RCLED is much narrower than the emission spectrum of regular LEDs (Schubert *et al.* 1992a; Hunt *et al.*, 1992, 1993). The spectral width of the RCLED emitted into a certain direction is given by the optical characteristics of the cavity. In contrast, the spectral width of a regular LED is about $1.8\,kT$, a value that is much wider than the RCLED emission spectrum. A comparison of a regular GaAs LED and a GaInAs

RCLED emission spectrum is shown in Fig. 15.6. Comparison of the spectra shows that the RCLED emission spectrum is a factor of about 10 narrower than the spectrum of the GaAs LED.

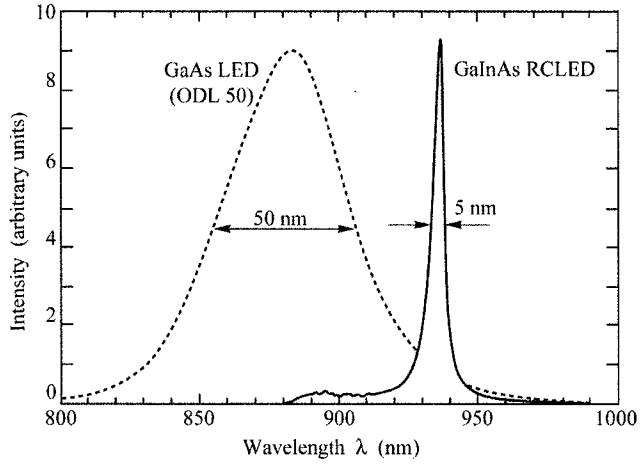

Fig. 15.6. Comparison of the emission spectra of a GaAs LED emitting at 870 nm (AT&T ODL 50 product) and a GaInAs RCLED emitting at 930 nm (after Hunt *et al.*, 1993).

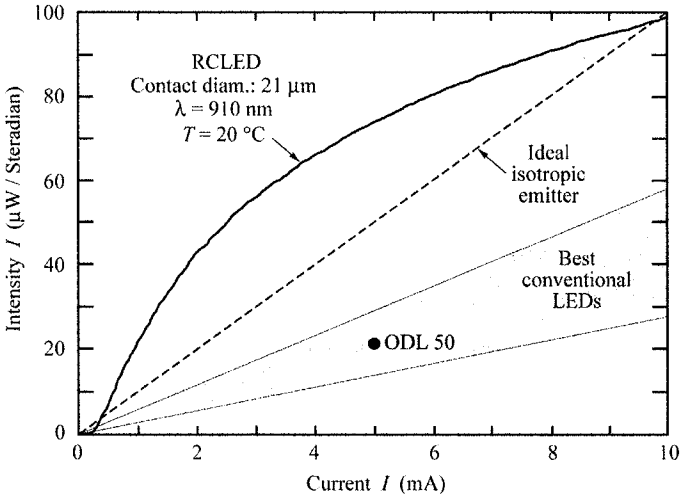

Fig. 15.7. Light-versus-current curves of a GaInAs/GaAs RCLED and of the *ideal isotropic emitter*. The ideal isotropic emitter is a hypothetial device emitting light isotropically with a quantum efficiency of 100%. The shaded region shows the intensity of the best conventional LEDs. The ODL 50 is a commercial LED product (after Schubert *et al.*, 1994).

A regular LED has little or no angle dependence of the emission spectrum. However, the reflective properties of DBRs and of cavities consisting of DBRs are angle-dependent. Consequently, the emission from an RCLED along a certain direction is narrower than that of a regular LED. Integrated over all directions, the RCLED has a broad emission spectrum.

A figure of merit for LEDs used in optical fiber communication systems is the photon flux

density emitted from the diode at a given current, which, for a given wavelength, can be characterized in terms of the unit microwatts per steradian. The optical power coupled into a fiber is directly proportional to the photon flux density.

The intensity of an RCLED as a function of the injection current is shown in Fig. 15.7. For comparison, the calculated intensity of the ***ideal isotropic emitter***, which is a hypothetical device, is also shown. The ideal isotropic emitter is assumed to have an internal quantum efficiency of 100% and the device is assumed to be clad by an anti-reflection coating providing zero reflectivity ($R = 0$) for all wavelengths emitted from the active region. If the photon emission inside the semiconductor is isotropic, then the optical power per unit current per unit solid angle normal to the planar semiconductor surface is given by

$$\frac{P_{\text{optical}}}{\Omega} = \frac{1}{4\pi\bar{n}^2}\frac{hc}{e\lambda} \tag{15.4}$$

where Ω represents the unit solid angle, $\bar{n}$ is the refractive index of the semiconductor, c is the velocity of light, e is the electronic charge, and λ is the emission wavelength in vacuum. Equation (15.4) is represented by the dashed line in Fig. 15.7. Neither the 100% internal quantum efficiency nor the hypothetical anti-reflection coating can be reproduced in practice for fundamental reasons. Therefore, the ideal isotropic emitter represents an upper limit for the intensity attainable with any conventional LED. Of course, even the best conventional LEDs have intensities lower than that of the ideal isotropic emitter. Also included in Fig. 15.7 is the ODL 50 GaAs LED, frequently used for optical fiber communication. All devices shown in Fig. 15.7 have planar light-emitting surfaces, and no lensing is used.

Figure 15.7 reveals that the RCLED provides unprecedented intensities in terms of both absolute values and slope efficiencies. The slope efficiency is 7.3 times the efficiency of the best conventional LEDs and 3.1 times the calculated efficiency of the ideal isotropic emitter. At a current of 5 mA, the intensity of the RCLED is 3.3 times that of the best conventional LEDs including the ODL 50. The high efficiencies make the RCLED well suited for optical interconnect and communication systems.

The higher spectral purity of RCLEDs reduces chromatic dispersion in optical fiber communications (Hunt *et al.*, 1993). The chromatic dispersion is directly proportional to the linewidth of the source. Since RCLEDs have linewidths 5–10 times narrower than conventional LEDs, chromatic dispersion effects, which dominate at wavelengths of 800–900 nm, are reduced as well. Hunt *et al.* (1993) showed that the bandwidth of RCLEDs is a factor of 5–10 higher than

that of conventional LEDs. An RCLED-versus-LED comparison in a transmission experiment is shown in Fig. 15.8. The results show the received signal after transmission lengths of 5 m and 3.4 km for the two devices. The fiber used is a graded-index multimode fiber with a core diameter of 62.5 μm. After a transmission length of 5 m, no marked difference is found for the two devices. However, a substantial difference is found after a transmission length of 3.4 km. Inspection of Fig. 15.8 reveals that the RCLED exhibits much less pulse broadening as compared to the conventional LED. This difference is due to reduced material dispersion for the RCLED.

Schubert *et al.* (1996) demonstrated the high-speed modulation capability of RCLEDs. Eye diagram measurements with a random bit pattern generator revealed wide-open eyes at 622 Mbit/s. Due to the small size of the current injected region, the parasitic capacitances of communication RCLEDs are small. It is expected that RCLEDs will be suitable for modulation frequencies exceeding 1 Gbit/s.

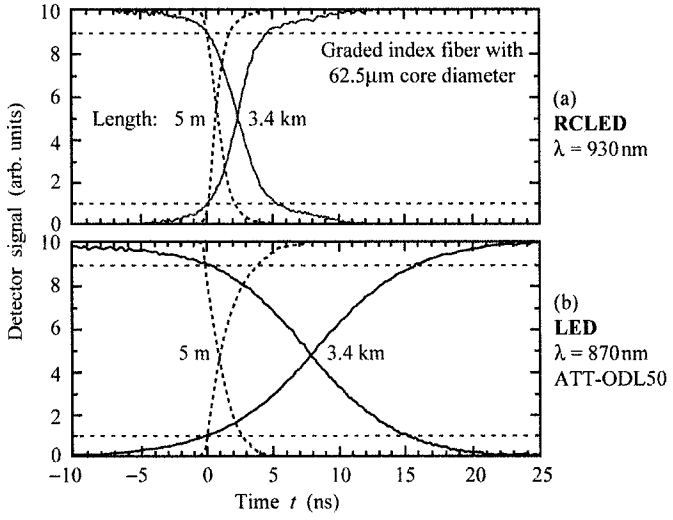

Fig. 15.8. Signal detected at the receiver end of a graded-index multimode fiber with a core diameter of 62.5 μm using (a) a GaInAs RCLED and (b) a GaAs LED source. After a short transmission distance of 5 m, no marked difference is found for the two sources. After a trans-mission distance of 3.4 km, the RCLED exhibits much less pulse broadening than the LED (after Hunt *et al.*, 1993).

15.4 AlGaInP/GaAs RCLEDs emitting at 650 nm

RCLEDs have also been demonstrated in the visible wavelength range using the AlGaInP material system (Streubel *et al.*, 1998; Whitaker, 1999; Wirth *et al.*, 2001, 2002). The AlGaInP material system is commonly used for high-brightness red, orange, and yellow emitters and can be grown lattice matched on GaAs substrates. The active region of RCLEDs is an AlGaInP/GaInP multiple-quantum well structure emitting at 650 nm. The RCLEDs are suited for

use in communication systems using plastic optical fibers. It is difficult to fabricate VCSELs in this wavelength range due to the unavailability of lattice-matched and transparent DBR materials with a large refractive-index contrast.

The basic structure of a top-emitting AlGaInP RCLED emitting at 650 nm is shown in Fig. 15.9. The device consists of an AlGaInP/GaInP MQW active region and AlGaInP cladding layers. The DBRs consist of AlAs/AlGaAs layers. The Al content in the AlGaAs layers of the DBR is chosen to be sufficiently high to make the DBR transparent to the light emitted by the active region. As a result, the index contrast of the AlAs/AlGaAs DBR layers is somewhat low.

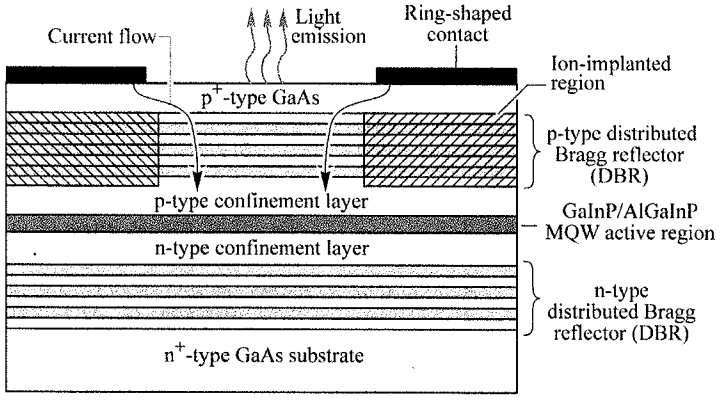

Fig. 15.9. Structure of a GaInP/AlGaInP/GaAs MQW RCLED emitting at 650 nm used for plastic optical fiber applications (after Whitaker, 1999)

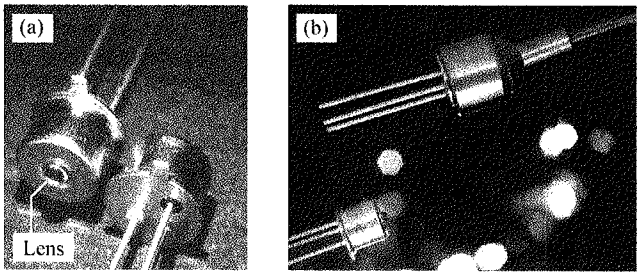

Fig. 15.10. (a) Packaged (TO package) RCLED emitting at 650 nm suited for plastic optical fiber applications. (b) Pig-tailed RCLED (courtesy of Mitel Corporation, Sweden, 1999).

The RCLED has a ring-shaped top contact configuration. The current is funneled into the center region of the ring using ion implantation to create an insulating region under the ring-shaped metalization. Hydrogen and, more frequently, oxygen implantation is used to render the semiconductor highly resistive. Note that the ion-implanted region is located in the p-type region

only and does not extend into the active region, thereby avoiding the creation of defects in the active region where they would act as luminescence killers.

Packaged RCLEDs in a lensed TO package and in a pig-tailed package are shown in Figs. 15.10 (a) and (b) (Mitel Corporation, 1999), respectively. The lens is used for beam collimation, thereby enhancing the coupling efficiency to fibers.

Three RCLEDs under current injection conditions are shown in Fig. 15.11 (Osram Opto Semiconductors Corporation). The picture shows that the emission pattern is directed towards the surface normal of the devices. The emission wavelength is 650 nm.

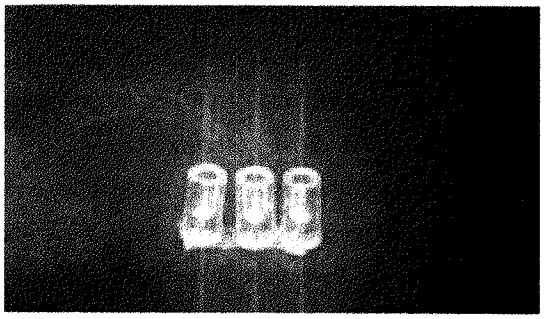

Fig. 15.11. AlGaInP/GaAs RCLEDs emitting at 650 nm. Note the forward-directed emission pattern similar to that of a semiconductor laser (courtesy of Osram Opto Semiconductors Corporation, Germany, 1999).

Optical spectra of a 650 nm RCLED and of a conventional LED injected at different current levels are shown in Fig. 15.12. The spectra are measured after the light is coupled into a plastic optical fiber. Thus, the magnitude of the spectra is a direct measure of the device efficiency *and* of the coupling efficiency. Inspection of the figure reveals several features. Firstly, the RCLED has a higher coupled peak power as well as integrated power than the LED. Secondly, the RCLED has a higher spectral purity than the LED.

Streubel *et al.* (1998) also reported that the emission spectrum was, at room temperature, intentionally blue-shifted with respect to the cavity resonance in order to improve the temperature stability of the RCLED output power. This cavity tuning results in a heart-shaped (double-lobed) emission pattern at room temperature, because the resonance wavelength of the cavity decreases for off-normal emission directions. As the temperature increases, the natural emission spectrum from the active region red-shifts, so that the cavity resonance (along the normal direction) has a better overlap with the natural emission spectrum. As a result, the temperature sensitivity of the RCLED is reduced. The natural emission spectrum red-shifts at a rate of about 0.5 nm/°C, whereas the cavity resonance shifts at only about one-tenth of that rate.

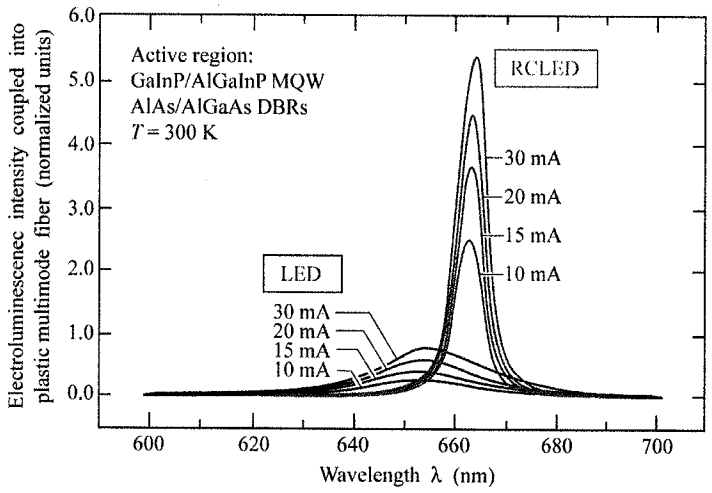

Fig. 15.12. Spectra of light coupled into a plastic optical fiber from a GaInP/AlGaInP MQW RCLED and a conventional GaInP/AlGaInP LED at different drive currents. Note the narrower spectrum and higher coupled power of the RCLED (after Streubel *et al.*, 1998).

15.5 Large-area photon recycling LEDs

Instead of devising ways to *reduce the lateral emission*, one could devise ways to *recycle* lateral emission, thereby redirecting the emission towards the top of the device. By reabsorbing the lateral emission, one can recapture the energy into the active region, giving it another chance to emit along the desired direction. Below, two examples of such devices are discussed.

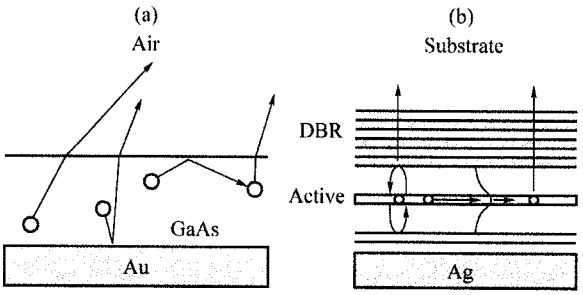

Fig. 15.13. Two approaches to photon recycling LEDs. (a) Bulk epilayer placed on top of gold. Most spontaneous emission that does not escape into air is reabsorbed and has a chance to emit again. (b) Microcavity designed with a waveguiding active region. Waveguided light is reabsorbed after some tens of micrometers, and has a chance to re-emit out of the top of the device.

The first example of such a device is an optically pumped semiconductor structure reported by Schnitzer *et al.* (1993). Consider the structure shown in Fig. 15.13 (a). The backside of a thin semiconductor layer is coated with gold. If one optically pumps the sample at low intensities, the active region remains absorbing. Most of the emission (about 95%) that hits the semiconductor–air interface will totally internally reflect, and stay within the semiconductor. Gold is a good reflector at infrared wavelengths. The semiconductor forming the active region is absorbing at the emission wavelength, so after some average absorption length, L_{abs}, the trapped light has a chance to re-emit.

This structure exhibited 72% external efficiency, which required a 99.7% internal quantum efficiency. The fabrication of the structure required the active epilayer to be etched and floated off its substrate. Note that the structure had no electrical contacts. The extraction efficiency of contactless structures is always higher compared with current-injection devices with contacts. An electrical device fabricated in this manner would probably have reliability problems due to the fragile nature of unsupported epitaxial films. A similar but more practical photon-recycling device was made by Blondelle *et al.* (1995).

The concept of photon recycling was used by De Neve *et al.* (1995) in a GaInAs/GaAs/AlGaAs RCLED. A simplified diagram of their structure is shown in Fig. 15.13 (b). If the graded-composition carrier confinement region is thick enough around the quantum wells, it also acts as a graded-index waveguide. De Neve *et al.* calculated that 30% of the light emitted by the active region goes into this waveguide mode. This is reabsorbed after some tens of micrometers, allowing the photons another chance to re-emit out of the top of the structure. In this way, about a 30% increase in external quantum efficiency was attained. The active region of quantum well RCLEDs is not thick enough to support a strongly guided optical mode. One might think that a strong waveguiding mode would take power away from the normal emission, but this does not appear to be the case. The energy tends to be at the expense of other high-angle modes instead, meaning that just modifying the waveguiding mode does little to change the external efficiency. Making use of this high-angle light by achieving photon recycling of the waveguiding emission is an attractive option.

One drawback to photon recycling is that it requires a device with large enough diameter that multiple reabsorption events can occur within the emitting area of the device. This makes such devices less attractive for fiber-optic communications, where small diameters couple better to fibers, especially when coupling lenses are used. Another drawback is that self-absorption necessarily increases the lifetime of the spontaneous emission, thereby slowing down the maximum modulation rate of the devices.

The device reported by De Neve *et al.* (1995) was shown to work with highest efficiency at large diameters. The authors were not targeting this RCLED for fiber communications. At high current densities, the carrier confinement in the quantum wells is reduced, and the efficiency decreases, so larger devices tend to be more efficient. Also, their device was resonant to the long-wavelength side of the natural emission peak, rather than at the peak. This shifts the maximum intensity of the main emission lobe to an off-normal angle, rather than being on axis, but it maximizes the total amount of emission into the main lobe. The Blondelle *et al.* (1995) and De

Neve *et al.* (1995) device is therefore designed for maximization of total emission from the top of the device, rather than for the specific needs of fiber coupling. Display devices and free-space communication devices benefit from this approach. The authors achieved an external quantum efficiency of 16%, compared with the theoretical 2% for an ideal planar emitter of the same index.

15.6 Thresholdless lasers

There have been a number of papers describing a thresholdless laser as a possible communications device (De Martini *et al.*, 1987). This would essentially be a light-emitting device that emitted most or all of its light into the fundamental spatial cavity mode. In this way, one can achieve the lasing condition of there being one photon in the cavity almost without gain. Let us denote the probability that light is emitted into the fundamental spatial cavity mode as β. If the β of the LED were almost 1, then the light-versus-current curve of the device would be linear, and *indistinguishable* from a laser with no threshold. A comparison of the light-versus-current for a conventional laser, a high-β laser, and a truly thresholdless laser is given in Fig. 15.14. If one envisions a thresholdless device as fabricated from a resonant-cavity pillar, there are a number of problems besides those of fabrication. Simply having a good sub-threshold intensity, giving only a small kink in the *L–I* curve between sub-threshold and lasing, is not good enough for a thresholdless laser. The output modulation of such a device would be extremely slow below threshold compared to the lasing regime. To enable lasing, there must be some gain, because the β will never be 1. For there to be gain, we must pump the active region past transparency first, since it is absorbing under no-pump conditions. This gain condition requires a certain carrier density, which, in fact, determines the threshold.

One can imagine a device such that all optical modes other than the fundamental are highly suppressed, and the internal quantum efficiency is nearly perfect. In this case, with even a small current, the carrier densities within the device would slowly build until the active region became transparent, and some light could get out through the fundamental optical mode. Such a device would have a very low threshold, but one would have to be careful not to ever drive the device below its threshold even momentarily, because of the long time required to build the necessary space charge inside the device for transparency. Also, if the fundamental emission was suppressed at low carrier densities, it is unlikely that the other modes would be suppressed by an even higher degree, which is what would be required not to lose the injected carriers. In fact, it is the difficulty in suppressing any side emission that makes semiconductor thresholdless lasers difficult if not impractical.

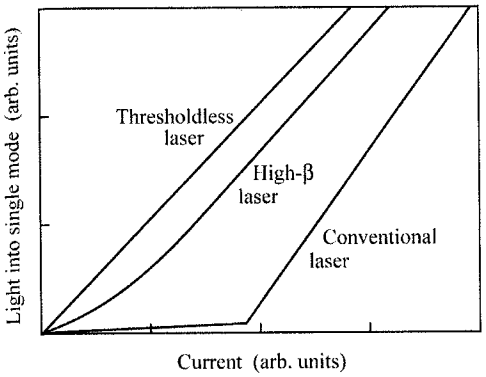

Fig. 15.14. Light-power-versus-current curves for single spatial-mode emission from (*i*) a conventional laser, (*ii*) a high β-factor laser, and (*iii*) a thresholdless laser. The conventional laser has a distinct current threshold. The high β-factor laser has a less distinct threshold. It would be noticeable in the spectrum and device modulation speed, however. A hypothetical thresholdless laser would have a β close to 1, and would somehow suppress all other lossy emission until the carrier density required for gain (or at least transparency) was achieved.

One could, of course, make a laser with a very small threshold by making the laser very small. The problem is that such a device would be capable of only a very small output power. For a hypothetical four-quantum-well single-mode LED, which does not rely on gain, but achieves a β close to 1, the current densities cannot be more than about 50 $\mu A/\mu m^2$ or 5 kA/cm^2. Using the formulas for β for a dielectric pillar ($\beta > 0.5$), and this current density, one can find that less than 2 μW could be emitted into a single mode for an RCLED pillar structure. This is clearly too small for high-speed communications in the 100–650 Mbit/s regime, where 10 μW is considered a minimum for an emitter. An RCLED with a very short carrier lifetime owing to extreme enhancement of the desired emission could have higher pump currents, but no semiconductor design can do this. If the device is a laser, higher powers could be drawn because of the reduced carrier lifetime, but the device sizes are incredibly small for real fabrication, or for any sort of heat dissipation.

In conclusion, semiconductor RCLEDs should remain devices larger than about 5 or 10 μm in diameter, and should remain multimode emitters. Semiconductor vertical-cavity lasers are best fabricated at sizes that make sense technologically, without regard to the β factor of the spontaneous emission. A high-β laser may not be desirable anyway, since the spontaneous emission will introduce excess noise into the emission.

15.7 Other RCLED devices

It is likely that the future of resonant-cavity LEDs and confined-photon emitters will involve new materials and applications from those currently used in communications and display systems. Spontaneously emitting confined-photon devices will always have competition from lasers, conventional LEDs, and other forms of devices. It is only a matter of time, however, before the right

materials combination at the right wavelengths, for the right application, will make commercial devices a reality. It is therefore worthwhile to mention other confined photonic LED material systems.

Wilkinson *et al.* (1995) fabricated an AlGaAs/GaAs thin-film emitter with metal mirrors on a Si substrate, emitting at 880 nm. Pavesi *et al.* (1996) fabricated porous silicon RCLEDs at 750 nm wavelength. Fisher *et al.*, (1995) investigated a conjugate polymer RCLED designed for 650 nm. Hadji *et al.* (1995) have realized CdHgTe/HgTe RCLEDs operating at a wavelength of 3.2 μm.

A structure of particular note is a GaAs/Al_xO_y RCLED (Huffaker *et al.*, 1995) operating at 950 nm, where the aluminum oxide in the output mirror was produced from AlAs by oxidation. This composition of output mirror allows the effective cavity length to remain small, maximizing the output enhancement in the RCLED. The back mirror of the structure was Ag. Another particularly interesting device is the broadly tunable RCLED by Larson and Harris (1995). The top mirror is a deformable membrane which can be moved by electrostatic forces. Tunable emission was shown from 938 to 970 nm.

15.8 Other novel confined-photon emitters

A complete discussion of other light-emitting structures that confine photons is beyond the scope of this chapter. It is useful, however, to discuss the properties of some confined-photon emitters. ***Photonic crystal*** or ***photonic bandgap structures*** or involve two- or three-dimensional photon confinement achieved by periodic patterning of the light-emitting active region or the material adjoining the active region. Examples of photonic crystal structures were given by Joannopoulos *et al.* (1995), Baba and Matsuzaki (1996), and Fan *et al.* (1997). Erchak *et al.* (2001) reported very encouraging results on photonic crystal LEDs, namely a six-fold enhancement of light extraction along the surface-normal direction.

Photonic crystal structures can consist of a series of rods or holes arranged in a regular pattern, such as a hexagonal close-packed array. The periodicity of the array can create an optical bandgap for lateral emission at certain emission energies and one or both polarizations. By suppressing the lateral emission, a structure consisting of rods will have a large bandgap for TM emission and a smaller bandgap for TE emission, but not at the same emission energies. However, if the emitting region had a dipole oriented mainly along the rods (such as in quantum well electron-to-light-hole recombination), the lateral emission could be efficiently suppressed. A structure consisting of patterned holes will have a smaller bandgap than that of the rod structure, but it has the advantage that it can have a true optical bandgap for both polarizations of light. Photonic crystal structures

either by themselves, or combined with a planar resonant cavity, enable a strong longitudinal emission enhancement.

Another confined-photon emitter is the ***microdisk laser*** (McCall *et al.*, 1992), which is fabricated as a thin dielectric disk that couples light out the edges of the disk. Lasing modes can be described by a mode number M, where $\exp(iM\phi)$ is the form of the electric field around the cylindrical disk. Because waves can propagate both ways, M can be positive or negative. The disk can be fabricated with a thickness such that the emission perpendicular to the disk is suppressed. Small disks will only support a few modes, and therefore can have a high spontaneous emission factor β. The Q of these modes are also high enough to achieve lasing. One attractive aspect of such disks is that the lasing emission occurs in the plane of the sample, from a very small device. This could be useful for integration of many photonic devices on a single wafer. However, the output is difficult to efficiently couple into waveguides and fibers, as it only couples evanescently. Advances have been made in improving the longevity, operating temperature range, and active-region passivation of such devices (Mohideen *et al.*, 1993). Room-temperature cw electrical pumping is still a problem, however.

References

Baba T. and Matsuzaki T., "GaInAsP/InP 2-dimensional photonic crystals" in *Microcavities and Photonic Bandgaps* edited by J. Rarity and C. Weisbuch, p. 193 (Kluwer Academic Publishers, Netherlands, 1996)

Blondelle J., De Neve H., Demeester P., Van Daele P., Borghs G., and Baets R. "16% external quantum efficiency from planar microcavity LED's at 940 nm by precise matching of the cavity wavelength" *Electron. Lett.* **31**, 1286 (1995)

De Martini F., Innocenti G., Jacobovitz G. R., and Mataloni P. "Anomalous spontaneous emission time in a microscopic optical cavity" *Phys. Rev. Lett.* **59**, 2955 (1987)

De Neve H., Blondelle J., Baets R., Demeester P., Van Daele P., and Borghs G. "High efficiency planar microcavity LEDs: Comparison of design and experiment" *IEEE Photonics Technol. Lett.* **7**, 287 (1995)

Erchak A. A., Ripin D. J., Fan S., Rakich P., Joannopoulos J. D., Ippen E. P., Petrich G. S., and Kolodziejski L. A. "Enhanced coupling to vertical radiation using a two-dimensional photonic crystal in a semiconductor light-emitting diode" *Appl. Phys. Lett.* **78**, 563 (2001)

Fan S., Villeneuve P. R., Joannopolous J. D., and Schubert E. F. "High extraction efficiency of spontaneous emission from slabs of photonic crystals" *Phys. Rev. Lett.* **78**, 3294 (1997)

Fisher T. A., Lidzey D. G., Pate M. A., Weaver M. S., Whittaker D. M., Skolnick M. S., and Bradley D. D. C. "Electroluminescence from a conjugated polymer microcavity structure" *Appl. Phys. Lett.* **67**, 1355 (1995)

Hadji E., Bleuse J., Magnea N., and Pautrat J. L. "3.2 μm infrared resonant cavity light emitting diode" *Appl. Phys. Lett.* **67**, 2591 (1995)

Huffaker D. L., Lin C. C., Shin J., and Deppe D. G. "Resonant cavity light emitting diode with an Al_xO_y/GaAs reflector" *Appl. Phys. Lett.* **66**, 3096 (1995)

Hunt N. E. J., Schubert E. F., Logan R. A., and Zydzik G. J. "Enhanced spectral power density and reduced linewidth at 1.3 μm in an InGaAsP quantum well resonant-cavity light-emitting diode" *Appl. Phys. Lett.* **61**, 2287 (1992)

Hunt N. E. J., Schubert E. F., Kopf R. F., Sivco D. L., Cho A. Y., and Zydzik G. J. "Increased fiber communications bandwidth from a resonant cavity light-emitting diode emitting at $\lambda = 940$ nm" *Appl. Phys. Lett.* **63**, 2600 (1993)

Hunt N. E. J., Schubert E. F., Sivco D. L., Cho A. Y., Kopf R. F., Logan R. A., and Zydzik G. J. "High efficiency, narrow spectrum resonant cavity light-emitting diodes" in *Confined Electrons and Photons* edited by E. Burstein and C. Weisbuch (Plenum Press, New York, 1995a)

Hunt N. E. J., Vredenberg A. M., Schubert E. F., Becker P. C., Jacobson D. C., Poate J. M., and Zydzik G. J. "Spontaneous emission control of Er^{3+} in Si/SiO_2 microcavities" in *Confined Electrons and Photons* edited by E. Burstein and C. Weisbuch (Plenum Press, New York, 1995b)

Joannopoulos J. D., Meade R. D., and Winn J. N. *Photonic Crystals* (Princeton University Press, Princeton NJ, 1995)

Kobayashi T., Segawa T., Morimoto A., and Sueta T., paper presented at the 43rd fall meeting of the Japanese Society of Applied Physics, Tokyo, Sept. (1982)

Larson M. C. and Harris Jr. J. S. "Broadly tunable resonant-cavity light emission" *Appl. Phys. Lett.* **67**, 590 (1995)

Lear K. L. and Schneider Jr. R. P. "Uniparabolic mirror grading for vertical cavity surface emitting lasers" *Appl. Phys. Lett.* **68**, 605 (1996)

McCall S. L., Levi A. F. J., Slusher R. E., Pearton S. J., and Logan R. A. "Whispering-gallery mode microdisk laser" *Appl. Phys. Lett.* **60**, 289 (1992)

Mitel Corporation, Sweden. Photograph of RCLED is gratefully acknowledged (1999)

Mohideen U., Hobson W. S., Pearton J., Ren F., and Slusher R. E. "GaAs/AlGaAs microdisk lasers" *Appl. Phys. Lett.* **64**, 1911 (1993)

Nakayama T., Itoh Y., and Kakuta A. "Organic photo- and electroluminescent devices with double mirrors" *Appl. Phys. Lett.* **63**, 594 (1993)

Osram Opto Semiconductors Corp., Germany. RCLED photograph is gratefully acknowledged (1999)

Pavesi L., Guardini R., and Mazzoleni C. "Porous silicon resonant cavity light emitting diodes" *Solid State Comm.* **97**, 1051 (1996)

Schnitzer I., Yablonovitch E., Caneau C., and Gmitter T. J. "Ultra-high spontaneous emission quantum efficiency, 99.7% internally and 72% externally, from AlGaAs/GaAs/AlGaAs double heterostructures" *Appl. Phys. Lett.* **62**, 131 (1993)

Schubert E. F., Wang Y.-H., Cho A. Y., Tu L.-W., and Zydzik G. J. "Resonant cavity light-emitting diode" *Appl. Phys. Lett.* **60**, 921 (1992a)

Schubert E. F., Vredenberg A. M., Hunt N. E. J., Wong Y. H., Becker P. C., Poate J. M., Jacobson D. C., Feldman L. C., and Zydzik G. J. "Giant enhancement of luminescence intensity in Er-doped Si/SiO_2 resonant cavities" *Appl. Phys. Lett.* **61**, 1381 (1992b)

Schubert E. F., Tu L. W., Zydzik G. J., Kopf R. F., Benvenuti A., and Pinto M. R. "Elimination of heterojunction band discontinuities by modulation doping" *Appl. Phys. Lett.* **60**, 466 (1992c)

Schubert E. F., Hunt N. E. J., Micovic M., Malik R. J., Sivco D. L., Cho A. Y., and Zydzik G. J. "Highly efficient light-emitting diodes with microcavities" *Science* **265**, 943 (1994)

Schubert E. F., Hunt N. E. J., Malik R. J., Micovic M., and Miller D. L. "Temperature and modulation characteristics of resonant cavity light-emitting diodes" *IEEE J. Lightwave Technol.* **14**, 1721 (1996)

Streubel K., Helin U., Oskarsson V., Backlin E., and Johanson A. "High-brightness visible (660 nm) resonant-cavity light-emitting diode" *IEEE Photonics Technol. Lett.* **10**, 1685 (1998)

Tu L. W., Schubert E. F., Zydzik G. J., Kopf R. F., Hong M., Chu S. N. G., and Mannaerts J. P. "Vertical cavity surface emitting lasers with semitransparent metallic mirrors and high quantum efficiencies" *Appl. Phys. Lett.* **57**, 2045 (1990)

Whitaker T. "Resonant cavity LEDs" *Compound Semiconductors* **5**, 32 (1999)

Wilkinson S. T., Jokerst N. M., and Leavitt R. P. "Resonant-cavity-enhanced thin-film AlGaAs/GaAs/AlGaAs LED's with metal mirrors" *Appl. Opt.* **34**, 8298 (1995)

Wirth R., Karnutsch C., Kugler S., and Streubel K. "High-efficiency resonant-cavity LEDs emitting at 650 nm" *IEEE Photonics Technol. Lett.* **13**, 421 (2001)

Wirth R., Huber W., Karnutsch C., and Streubel K. "Resonators provide LEDs with laser-like performance" *Compound Semiconductors* **8**, 49 (2002)

Yokoyama H. "Physics and device applications of optical microcavities" *Science* **256**, 66 (1992)

22

Optical communication

LEDs are used in communication systems transmitting low and medium data rates (< 1 Gbit/s) over short and medium distances (< 10 km). These communication systems are based on either *guided light waves* (Keiser, 1999; Neyer *et al.*, 1999; Hecht, 2001; Mynbaev and Scheiner, 2001; Kibler *et al.*, 2004) or *free-space waves* (Carruthers, 2002; Heatley *et al.*, 1998; Kahn and Barry, 2001). In guided-wave communication, individual optical fibers or fiber bundles are used as the transmission medium and LED-based optical communication links are limited to distances of a few kilometers. Optical fiber systems include *silica* and *plastic* optical fibers. Free-space communication is usually limited to a room, even though longer distances are possible. In this chapter we discuss the characteristics of transmission media used for LED communication.

22.1 Types of optical fibers

The cross section of optical fibers consists of a circular core region surrounded by a cladding region. The core region has a higher refractive index than the cladding region. Typically, the core refractive index is about 1% higher than the cladding refractive index. Light propagating in the core is guided inside the core by means of *total internal reflection*. The condition of total internal reflection can be inferred from Snell's law. A light ray is *totally internally reflected* whenever it is incident at the core–cladding boundary. In a ray-optics picture, light rays propagating inside the core follow a *zigzag path*.

There are three types of optical fibers used in communication systems. These types are the (*i*) *step-index multimode* fiber, (*ii*) *graded-index multimode* fiber, and (*iii*) *single-mode* fiber. The three types of fibers are shown in Fig. 22.1 along with the refractive index profiles.

Step-index multimode fibers have a relatively large core diameter. Typical core diameters are 50, 62.5, and 100 μm for silica fibers used in communication systems. Plastic optical fibers have larger core diameters, typically 1 mm. An important advantage of multimode fibers is *easy coupling* of the light source to the fiber. Usually, a ± 5 μm accuracy of alignment is sufficient for

multimode fibers with a core diameter of 50 μm. The main disadvantage of multimode fibers is the occurrence of *modal dispersion.*

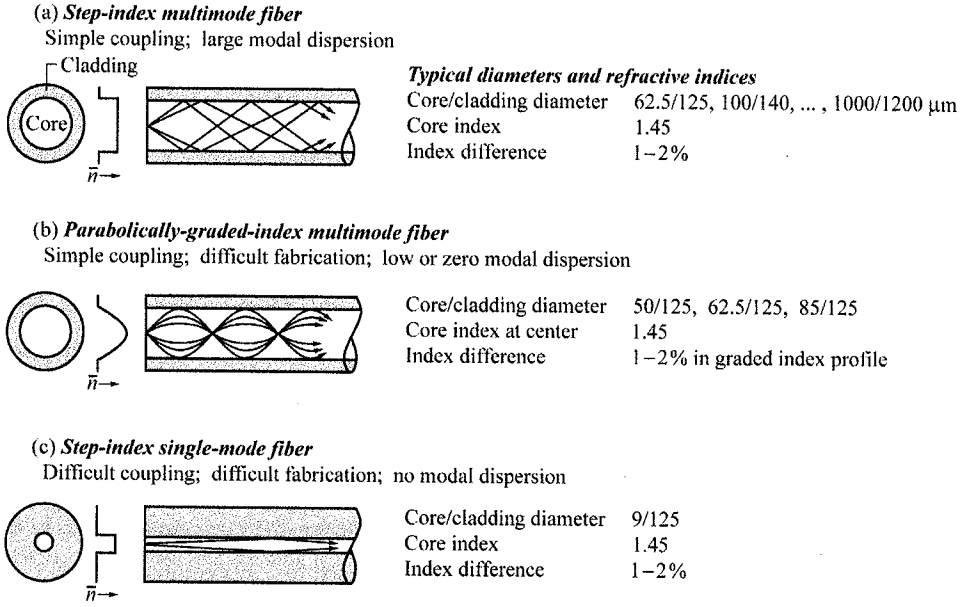

Fig. 22.1. (a) Step-index multimode fibers allow for the propagation of several optical modes. (b) Parabolically graded-index multimode fibers allow for the propagation of several modes with similar propagation constant. Graded-index multimode fibers have a lower modal dispersion than step-index multimode fibers. (c) Step-index single-mode fibers have a small core diameter and no modal dispersion.

Because the core diameter in multi-mode fibers is much larger than the operating wavelength, several optical modes can propagate in the waveguide. These optical modes have different propagation constants so that different modes arrive at the end of the fiber at different times, even if they were launched at the same time. This leads to a broadening of the optical pulse and limits the maximum bit rate that can be transmitted over a fiber of a given length.

Modal dispersion is reduced by *graded-index* multimode fibers. Graded-index multimode fibers have a parabolically graded core index leading to a reduction in modal dispersion.

Single-mode fibers have such a small core diameter that only a single optical mode can propagate in the fiber. Typical single-mode core diameters are 5–10 μm. The main advantage of single-mode fibers is the *lack of modal dispersion.* The main disadvantage of single-mode fibers is *difficult coupling* due to the small core diameter. A small core diameter requires light sources

with high brightness such as lasers. However, LEDs, in particular edge-emitting LEDs and superluminescent LEDs are also occasionally used with single-mode fibers. Coupling of light into single-mode fibers requires precise alignment with tolerances of a few micrometers.

If the *optical power* to be transmitted over an optical fiber is of prime interest, the core diameter should be as large as possible and the core–cladding index difference should also be as large as possible. Specialty fibers with core diameters of > 1 mm are available. Such fibers are not suitable for communication applications due to the large modal dispersion.

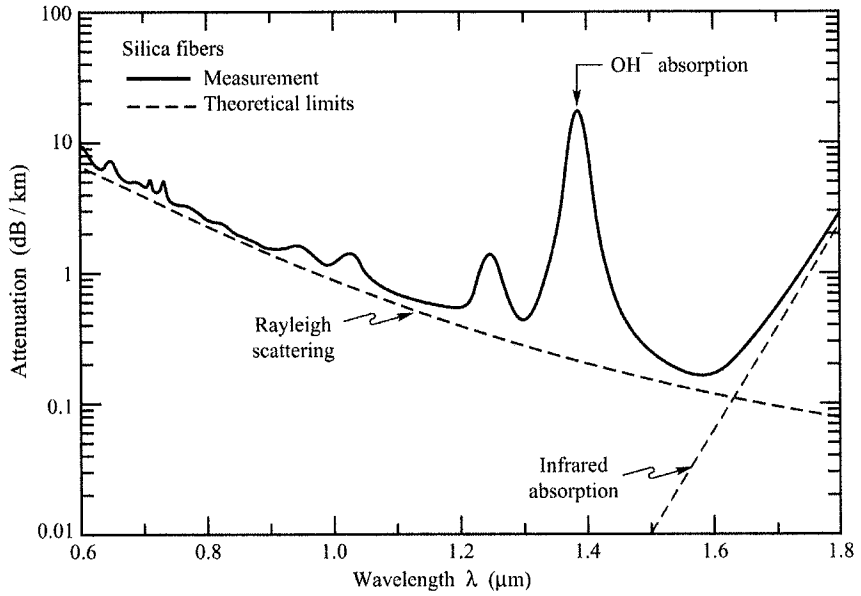

Fig. 22.2. Measured attenuation in silica fibers (solid line) and theoretical limits (dashed lines) given by Rayleigh scattering in the short-wavelength region, and by molecular vibrations (infrared absorption) in the infrared spectral region.

22.2 Attenuation in silica and plastic optical fibers

Silica (SiO_2) has excellent optical properties including great long-term stability. A large variety of glasses and fibers are available. The attenuation of silica fibers is shown in Fig. 22.2. Inspection of Fig. 22.2 reveals that a minimum loss of 0.2 dB occurs at a wavelength of 1.55 μm.

There are several optical "windows" for communication over silica fibers. These communication windows are at 0.85, 1.3, and 1.55 μm. The 0.85 μm communication window is suitable for communication with GaAs-based LEDs and lasers. However, this window is limited

to short distances due to the material dispersion and to the high attenuation of silica fibers at that wavelength. The 1.3 μm communication window is also suited for communication with LEDs and lasers. This window has relatively low loss and zero dispersion, allowing for high-bit-rate transmission, in particular in graded-index and single-mode fibers. The 1.55 μm communication window is characterized by the lowest loss of all three windows. Consequently, this window is used for long-distance high-bit-rate communication. To allow for high bit rates, single-mode fibers must be used. Since it is difficult to efficiently couple light emerging from an LED into a single-mode fiber, lasers are preferred over LEDs at 1.55 μm.

Plastic optical fibers are becoming increasingly popular for short-distance communication (Neyer *et al.*, 1999; Kibler *et al.*, 2004). However, plastic fibers have losses that are about 1 000 times greater than the losses in silica fibers. Therefore, the transmission distances are limited to just a few meters to a few hundred meters, e.g. for communication within an automobile (Kibler *et al.*, 2004) or airplane.

The attenuation in plastic fibers is shown in Fig. 22.3. The preferred communication window of plastic fibers is at 650 nm, where the loss is of the order of 0.1–0.2 dB per meter. At even shorter wavelengths, the attenuation in plastic fibers decreases. However, the material dispersion increases, thus making the 650 nm wavelength the preferred communication wavelength in plastic optical fibers.

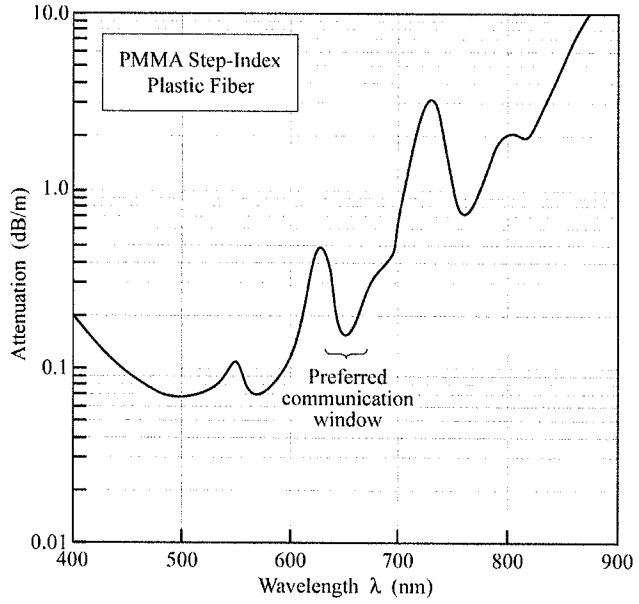

Fig. 22.3. Attenuation of a PMMA step-index plastic optical fiber. At 650 nm, the preferred communication wavelength, the attenuation is about 150 dB/km (after data sheet of Toray Industries Ltd., 2002).

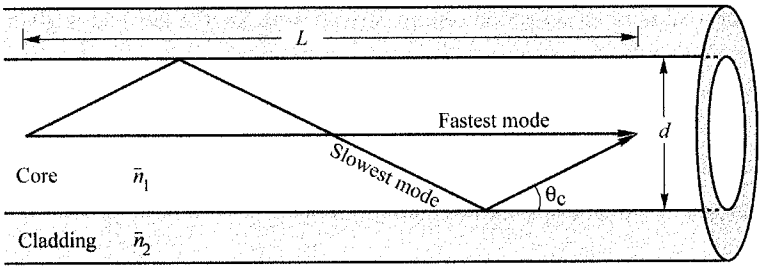

Fig. 22.4. Geometry used for calculation of the modal dispersion in a multimode fiber waveguide.

22.3 Modal dispersion in fibers

Modal dispersion occurs in multimode fibers that have a larger core diameter or a larger index difference between the core and the cladding than single-mode fibers. Typical core diameters range from 50 to 1 000 μm for multimode fibers and 5 to 10 μm for single-mode fibers. In the ray optics model, *different optical modes* correspond to light rays propagating at *different angles* in the core of the waveguide. The derivation of propagation angles in multimode fibers would go beyond the scope of this chapter. Here an approximate calculation will be performed to obtain the modal dispersion.

Consider a fiber waveguide with refractive indices of the core and cladding of $\bar{n}_1$ and $\bar{n}_2$, respectively. Assume that the waveguide supports the propagation of more than one optical mode. Two of these modes are shown schematically in Fig. 22.4. Owing to the difference in optical path length, the mode with the smaller propagation angle θ will arrive earlier at the end of the multimode fiber. The ***modal dispersion*** is the time delay between the fastest and the slowest optical mode normalized to the length L of the waveguide.

In the calculation, assume that the phase and group velocity are given by $v_{ph} = c/\bar{n}_1 \approx v_{gr}$. The fastest mode has the smallest propagation angle and we approximate the smallest angle by $\theta_{m=0} \approx 0°$. The slowest mode has the largest propagation angle and we approximate the largest angle by $\theta_m \approx \theta_c$, where θ_c is the critical angle of total internal reflection. This approximation can be made without loss of accuracy for multimode fibers which carry many modes.

The propagation times for the fastest and slowest modes per unit length of the fiber are given by

$$\tau_{fast} = \frac{L}{c/\bar{n}_1} \qquad \tau_{slow} = \frac{L/\cos\theta_c}{c/\bar{n}_1} \tag{22.1}$$

where the critical angle for total internal reflection can be derived from Snell's law and is given by

$$\theta_c = \arccos\left(\bar{n}_2 / \bar{n}_1\right). \tag{22.2}$$

The time delay per unit length, or modal dispersion, is then given by

$$\frac{\Delta\tau}{L} = \frac{\tau_{slow} - \tau_{fast}}{L} = \frac{n_1}{c}\left(\frac{1}{\cos\theta_c} - 1\right). \tag{22.3}$$

A waveguide supporting *many* modes has a large time delay between the fastest and slowest modes. Thus modal dispersion increases with the number of optical modes supported by the waveguide.

Exercise: ***Modal dispersion in waveguides***. Calculate the time delay between the slowest and the fastest modes, and the maximum possible bit rate for a 1 km long multimode fiber waveguide with core refractive index $\bar{n}_1 = 1.45$ and cladding refractive index $\bar{n}_2 = 1.4$.

Solution: Using Snell's law (Eq. 22.2), one obtains $\theta_c \approx 15°$. The time delay calculated from Eq. (22.3) amounts to $\Delta\tau = 170$ ns. The minimum time required to transmit one bit of information is given by $\Delta\tau$. This yields an approximate maximum bit rate of $f_{max} = 1/170$ ns $= 5.8$ Mbit/s. The calculation shows that modal dispersion can be a significant limitation in optical communication. Graded-index multimode fibers or single-mode fibers are therefore required for high-speed communication systems.

22.4 Material dispersion in fibers

Material dispersion is another mechanism limiting the capacity of optical fibers. Material dispersion is due to the dependence of the refractive index on the wavelength. Figure 22.5 shows, as a function of wavelength, the phase refractive index and the group refractive index of silica. The indices are defined as

$$\bar{n} = \frac{c}{v_{ph}} \qquad \text{(phase refractive index)} \tag{22.4}$$

and

$$\bar{n}_{gr} = \frac{c}{v_{gr}} \qquad \text{(group refractive index)} \tag{22.5}$$

where v_{ph} and v_{gr} are the phase and group velocity in silica, respectively. The ***phase refractive index*** and the ***group refractive index*** are related by

$$\bar{n}_{gr} = \bar{n} - \lambda \frac{d\bar{n}}{d\lambda} = \bar{n} - \lambda_0 \frac{d\bar{n}}{d\lambda_0} . \tag{22.6}$$

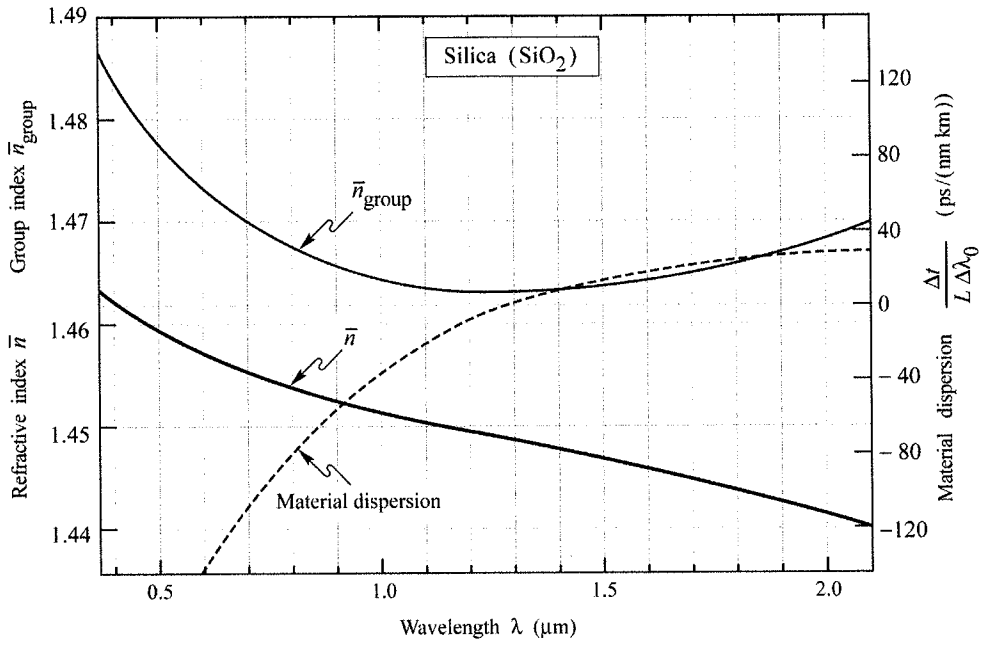

Fig. 22.5. Refractive index, group index, and material dispersion of a silica fibers for an optical signal spectral width $\Delta\lambda_0$ in vacuum. The material dispersion of regular silica fibers is zero at $\lambda = 1.3$ μm.

If the fiber is dispersive, the difference in group velocity between the "slowest color" and the "fastest color" of the optical signal is given by

$$\left|\Delta v_{gr}\right| = \frac{c}{\bar{n}_{gr}^2} \frac{d\bar{n}_{gr}}{d\lambda} \Delta\lambda \tag{22.7}$$

where $\Delta\lambda$ is the spectral width of the optical signal.

The time delay between the leading edge and the trailing edge of an optical signal after traveling in the fiber for a length L, called the ***material dispersion***, is given by

$$\Delta\tau = \frac{L}{v_{gr}^2} \Delta v_{gr} = \frac{L}{c} \frac{d\bar{n}_{gr}}{d\lambda} \Delta\lambda = \frac{L}{c} \frac{d\bar{n}_{gr}}{d\lambda_0} \Delta\lambda_0 . \tag{22.8}$$

The material dispersion is measured in ps/(nm km) and it is illustrated for silica fibers in Fig. 22.5. LEDs have a broad emission linewidth. Therefore material dispersion is, along with modal dispersion, the bandwidth-limiting factor in optical fiber communication systems operated with LEDs.

Exercise: ***Material dispersion in waveguides.*** Derive Eqs. (22.6) and (22.7). Why does material dispersion have a much smaller significance for semiconductor lasers than for LEDs?

Substantial material dispersion exists in plastic fibers at all wavelengths of interest. These wavelengths are the local loss minimum at 650 nm and the low-loss region of 500–600 nm. The material dispersion is given in Table 22.1. The data indicates that 650 nm is the wavelength of least dispersion, making 650 nm the preferred communication wavelength in plastic optical fibers.

Table 22.1. Material dispersion in PMMA plastic optical fibers (courtesy of R. Marcks von Wurtemberg, *Mitel* Corporation, 2000).

Wavelength	525 nm	560 nm	650 nm
Material dispersion	700 ps/(nm km)	500 ps/(nm km)	320 ps/(nm km)

Exercise: ***Comparison of material and modal dispersion.*** Consider a 62.5 μm core diameter multimode step-index fiber of 3 km length with a core index of $\overline{n}_1 = 1.45$ and a cladding index of $\overline{n}_2 = 1.4$. Assume that the fiber inputs come from either an LED or a laser emitting at 850 nm. Assume that the LED and the laser have a linewidth of 50 and 5 nm, respectively. Calculate the material and the modal dispersion for each case and explain the result.

22.5 Numerical aperture of fibers

Owing to the requirement of total internal reflection, the only light rays that can propagate losslessly in the core of an optical fiber are those that have a propagation angle smaller than the critical angle for total internal reflection. Light rays for which the propagation angle is too large will consequently not couple into the fiber. Here we consider the coupling of light from an LED light source into an optical fiber. We assume that the fiber end has a polished planar surface normal to the optical axis of the fiber, as shown in Fig. 22.6.

As a consequence of the requirement of total internal reflection, only a range of angles will be "accepted" by the fiber for lossless propagation. Outside the ***acceptance angle*** range, light

rays will be refracted into the cladding layer where they will incur losses.

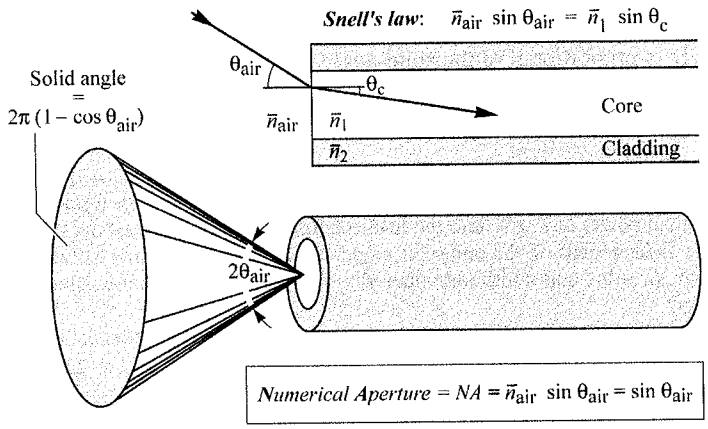

Fig. 22.6. Illustration of the *numerical aperture* (*NA*) of a fiber. For example, the light acceptance angle in air is $\theta_{air} = 11.5°$ for a numerical aperture of $NA = 0.2$.

The range of allowed angles can be inferred from Snell's law. As illustrated in Fig. 22.6, the maximum angle for acceptance in the fiber is given by

$$\bar{n}_{air} \sin\theta_{air} = \bar{n}_1 \sin\theta_c \,. \tag{22.9}$$

Since the refractive index of air is approximately unity, the maximum acceptance angle in air is given by

$$\theta_{air} = \arcsin(\bar{n}_1 \sin\theta_c). \tag{22.10}$$

The maximum acceptance angle defines a cone of allowed angles, as shown in Fig. 22.6. Light rays incident on the core of the optical fiber with propagation angles within the cone can propagate without loss.

Another way to express the acceptance cone is the ***numerical aperture*** of the fiber. The numerical aperture (*NA*) is defined as

$$NA = \bar{n}_1 \sin\theta_c = \bar{n}_{air} \sin\theta_{air} = \sin\theta_{air} \approx \theta_{air} \tag{22.11}$$

where the approximation $\sin\theta_{air} \approx \theta_{air}$ is valid for *small* numerical apertures. Typical *NA*s for silica single-mode fibers are 0.1 and typical *NA*s for silica multimode fibers are 0.15–0.25. Plastic optical fibers can have higher *NA*s, typically 0.2–0.4.

The solid angle corresponding to a certain *NA* is given by

$$\text{Solid angle} = \Omega = 2\pi(1-\cos\theta_{air}) = 2\pi\left[1-\cos(\arcsin NA)\right] \approx \pi NA^2 \qquad (22.12)$$

where the small-angle approximations $\sin\theta_{air} \approx \theta_{air}$ and $\cos\theta_{air} \approx 1 - (1/2)\theta_{air}^2$ have been used. The power emitted by an LED is proportional to the solid angle. Thus the power coupled to an LED is proportional to the *NA squared* of the fiber in the small-angle approximation.

Exercise: ***Coupling efficiency of a fiber butt-coupled to an LED.*** Consider an LED with a point-like emission region that emits an optical power of 1 mW into the hemisphere. For simplicity, assume that the intensity emitted by the LED is independent of the emission angle. What is the maximum acceptance angle of a single-mode fiber with $NA = 0.1$ and multimode fiber with $NA = 0.25$? What is the power that can be coupled into the two fibers?

Solution: The maximum acceptance angles of the single-mode and multimode fibers in air are $\theta_{air} = 5.7°$ and 14.5°, respectively. The solid angle defined by an acceptance angle θ_{air} is given by $\Omega = 0.031$ and 0.20 for the single-mode and multimode fiber, respectively. Since the entire hemisphere has a solid angle of 2π, the power coupled into the single-mode and multimode fibers is given by 0.0049 and 0.032 mW, respectively.

22.6 Coupling with lenses

The low coupling efficiency of LEDs to optical fibers can be improved with convex lenses, if the light-emitting region of the LED is smaller than the optical fiber core. In this case, the light-emitting region can be imaged on the fiber core, thereby reducing the angle of incidence. The light source is *adapted* to the *NA* of the fiber ("*NA-matching*").

A convex lens can produce an image with height I of a light-emitting object with height O. If the image is larger than the object, the angles of the light incident from the lens on the image are less divergent than the light emanating from the object towards the lens. The *smaller divergence* obtained for *magnified* images allows one to increase the coupling efficiency to fibers. The principle of coupling with a convex lens is shown in Fig. 22.7.

The condition for a focused image (minimum image size) is given by the lens equation

$$\frac{1}{d_O} + \frac{1}{d_I} = \frac{1}{f} \qquad (22.13)$$

where d_O and d_I are the distances of the object and the image from the lens, respectively, and f is the focal length of the lens.

The magnification of the image of the LED light source on the core of the fiber is given by

$$M = \frac{I}{O} = \frac{d_I}{d_O} . \tag{22.14}$$

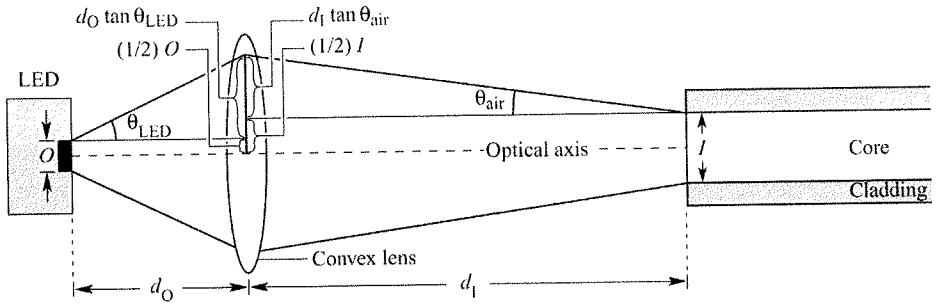

Fig. 22.7. Schematic illustration of coupling with a lens by imaging the light-emitting region of an LED onto the core of an optical fiber. The LED has a circular emission region with diameter O (Object). The emission region is imaged onto the fiber core with diameter I (Image) using a convex lens with focal length f.

As shown in Fig. 22.7, it is

$$\tfrac{1}{2}O + d_O \tan\theta_{LED} = \tfrac{1}{2}I + d_I \tan\theta_{air} . \tag{22.15}$$

If the LED and the core of the optical fiber are much smaller than the diameter of the lens and if the angles are relatively small, then Eq. (22.15) can be approximated by

$$\theta_{LED} = \frac{d_I}{d_O}\theta_{air} = \frac{I}{O}\theta_{air} . \tag{22.16}$$

Since d_I is larger than d_O, the acceptance angle for light emanating from the LED is *larger* than that of the fiber, implying *increased* coupling efficiency. Thus, we can define the numerical aperture of the LED, NA_{LED}, which defines the angle of light emanating from the LED that is accepted by the fiber. Using Eq. (22.14) and the small-angle approximation for NA, NA_{LED} is given by

$$NA_{LED} = \frac{I}{O} NA . \tag{22.17}$$

Since the coupling efficiency is proportional to NA^2 (see Eq. 22.12), the coupling efficiency is increased to

$$\text{Coupling efficiency} \propto NA_{\text{LED}}^2 = \left[(I/O)\,NA\right]^2 . \tag{22.18}$$

The result shows that high coupling efficiencies are obtained for LEDs with small-diameter light-emitting regions, large fiber-core diameters, and large-*NA* fibers.

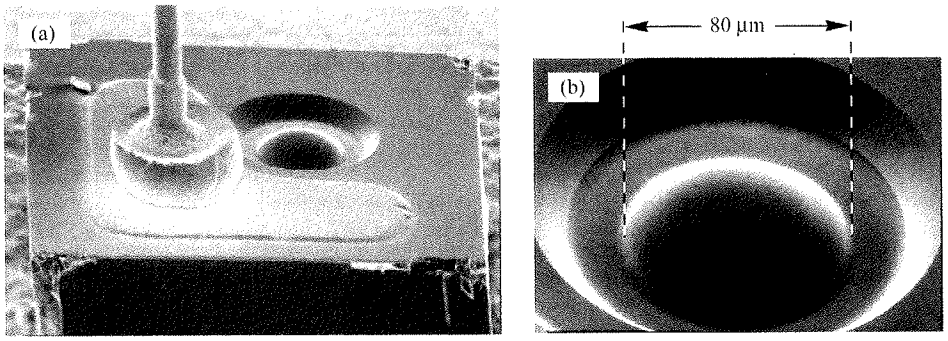

Fig. 22.8. (a) Commercial communication LED chip with integrated lens. (b) Detailed picture of the lens etched by a photochemical process into the GaAs substrate (AT&T ODL product line, 1995).

Lensed LEDs are frequently used in communication applications. A micrograph of an LED with a monolithically integrated lens is shown in Fig. 22.8. The light-emitting region of the LED is 20 μm and the lens shown in Fig. 22.8 has a diameter of about 80 μm.

Exercise: ***Coupling efficiency of a fiber coupled to an LED with a lens.*** Consider an LED circular emission region with diameter 20 μm coupled to a silica multimode fiber with NA = 0.2 and a core diameter of 62.5 μm. The LED emits a power of 1 mW into the hemisphere lying above the planar LED surface. For simplicity, assume that the LED emission intensity is independent of the emission angle. What is the maximum power that can be coupled into the multimode fiber?

Solution: Improved coupling can be obtained by imaging the LED emission region on to the core of the optical fiber. For maximum coupled power, a convex lens with magnification M = 62.5 μm / 20 μm = 3.125 can be used. Using the lens, the acceptance angle of the fiber is increased from $\theta_{\text{air}} = 11.5°$ to $\theta_{\text{LED}} = 35.9°$. The solid angle defined by the LED acceptance angle θ_{LED} is given by $\Omega = 1.19$. Since the LED emits 1 mW into the entire hemisphere (with solid angle $\Omega = 2\pi$), the power coupled into the fiber is given by 0.189 mW.

22.7 Free-space optical communication

Free-space optical communication (Carruthers, 2002; Heatley *et al.*, 1998; Kahn and Barry, 2001) is suitable for low to medium bit rates. The most common application of free-space optical

communication is the remote control of consumer appliances such as stereos and television sets. Other applications are the remote control of automobile door locks and the cordless interface between computers and peripheral devices such as a mouse, keyboard, and printer.

Free-space optical communication is limited to line-of-sight applications since obstacles such as walls and floors will block the path of light. Furniture may also block the path of light. However, a light beam may be reflected from the ceiling so that communication may still be possible even if there is no direct line of sight connection between the optical transmitter and the receiver.

The wavelength of choice for free-space optical communication is the near infrared. GaAs LEDs emitting with good efficiency are readily available. Infrared light is preferred over visible light sources because the former does not provide a distraction to anyone near the optical transmitter.

Eye safety considerations limit the maximum power of optical transmitters. At a wavelength of 870 nm, the optical power is limited to typically a few mW. Other wavelengths, such as 1500 nm, allow for higher optical powers. The 1 500 nm wavelength range is termed "*eye safe*", since the cornea absorbs 1 500 nm light, thus preventing light from reaching the sensitive retina. The wavelength 1 500 nm thus allows for higher optical powers than 870 nm sources.

If we restrict our considerations to small distances, the transmission medium air can be considered to be totally lossless. However, the optical signal strength decreases for uncollimated light beams due to spatial divergence. For *isotropic emitters*, the intensity decreases with the square of the radius, i.e.

$$I = P/(4\pi r^2) \tag{22.19}$$

where P is the optical power emitted by the source and r is the distance from the source. The decrease in intensity thus has a very different dependence compared with the intensity in fiber communication.

The rapidly decreasing intensity limits the maximum range of optical communication. Collimated light beams can overcome this problem. Transmission distances of several km are possible without significant loss provided that atmospheric conditions are good, i.e. in the absence of fog or precipitation. Semiconductor lasers are used for such collimated transmission systems due to the ability to form collimated beams with very little spatial dispersion.

Multipath distortion or ***multipath time delay*** severely limits the data rate in free-space optical communication systems. A schematic illustration of multipath distortion is shown in

Fig. 22.9. A light beam emanating from the optical transmitter may take several different paths from the transmitter to the receiver. This is especially true for rooms with high-reflectivity surfaces such as white ceilings, walls, or mirrors. As an approximate rule, the longest path is assumed to be twice as long as the shortest path between the transmitter and the receiver. This approximate rule leads to a multipath distortion time delay of

$$\Delta\tau = L/c \tag{22.20}$$

where L is the transmitter–receiver distance and c is the velocity of light. The maximum data rate is then limited to

$$f_{\max} \approx 1/\Delta\tau \, . \tag{22.21}$$

For a room size of 5 m, the multipath delay is about $\Delta\tau = 17$ ns. Thus the data rate will be limited to about 60 MHz.

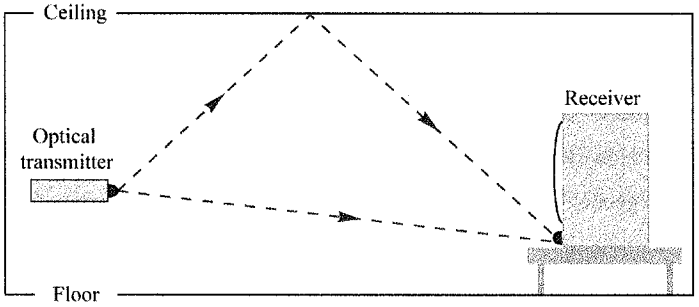

Fig. 22.9. Illustration of multipath distortion of a free-space optical signal, which limits the maximum data rate of the signal.

Another limitation of free-space optical communication is the detector noise. Sunlight and incandescent light sources have strong emission in the infrared. Thus a large DC photocurrent is generated in the detector, especially under direct sunlight conditions. The detector noise can be reduced by limiting the bandwidth of the receiver system. By reducing the bandwidth of the receiver system, and thereby also the system data rate, the detector noise is reduced, since the noise spectrum is much wider than the system bandwidth.

The detector noise due to ambient light sources can also be reduced by using optical band-pass filters, long-wavelength-pass filters, or a combination of both filters. Such filters prevent unwanted ambient light from reaching the detector.

References

Carruthers J. B. "Wireless infrared communications" in *Wiley Encyclopedia of Telecommunications* edited by J. G. Proakis (John Wiley and Sons, New York, 2002)

Heatley D. J. T., Wisely D. R., Neild I., and Cochrane P. "Optical wireless: the story so far" *IEEE Comm. Mag.* **36**, 72 (1998)

Hecht J. *Understanding Fiber Optics* (Prentice Hall, Upper Saddle River, New Jersey, 2001)

Kahn J. M. and Barry J. R. "Wireless infrared communications" *Proc. IEEE* **85**, 265 (2001)

Keiser G. *Optical Fiber Communications* 3rd edition (McGraw-Hill, New York, 1999)

Kibler T., Poferl S., Böck G., Huber H.-P., and Zeeb E. "Optical data buses for automotive applications" *IEEE J. Lightwave Technol.* **22**, 2184 (2004)

Mynbaev D. K. and Scheiner L. L. *Fiber-Optic Communications Technology* (Prentice Hall, Upper Saddle River, New Jersey, 2001)

Neyer A., Wittmann B., and Jöhnck M. "Plastic-optical-fiber-based parallel optical interconnects" *IEEE J. Sel. Top. Quantum Electron.* **5**, 193 (1999)